Research Article | Vol. 32, No. 17 / 12 Aug 2024 / Optics Express 29030
Optics EXPRESS

Optical theorem in the 3-D scattering from a locally perturbed lossless or lossy thin dielectric plate: silver disk-sealed hole analysis

MARIO LUCIDO[1] AND OLEKSANDR I. NOSYCH[2,*]

[1]Department of Electrical and Information Engineering, University of Cassino and Southern Lazio, Cassino 03043, Italy
[2]Laboratory of Micro and Nano-Optics, Institute of Radio-Physics and Electronics NASU, Kharkiv 61085, Ukraine
*anosich@yahoo.com

Abstract: This paper is aimed at devising a new optical theorem formulation for the 3-D plane-wave scattering from an infinite resistive plane and, more generally, a thin dielectric plate with a finite-size inhomogeneity shaped as a hollow or sealed hole. This formulation is further modified to cover the case of the plane guided wave scattering from the same inhomogeneity. For the lossless plane, the diffracted field combines a classical outgoing spherical wave, satisfying the Silver-Muller radiation condition, with an outgoing cylindrical guided wave supported by the plane; the power absorbed in the lossy filling is finite. When a lossy plane is involved, a complication appears: the total absorbed power is infinite. However, a change in the inhomogeneity characteristics perturbs the absorbed power density, thus suggesting the perturbative absorption analysis. After developing the analytical procedure for the resistive plane case and the corresponding generalization to the thin dielectric plate case, we illustrate the significance of the new optical theorem by the numerical analysis of the visible-light scattering from a dielectric plate with a circular nanosize hole sealed with a silver disk. Our analysis uses the in-house code having mathematically guaranteed convergence; it reveals the scattering and absorption resonances on the plasmon modes of the silver nanodisk. The derived optical theorem allows us to see that, in the resonances, the power carried by the guided waves can be comparable to the power scattered into the free space.

1. Introduction

The Optical Theorem (OT) has quite a long history [1] and features in many dozens of publications across a variety of disciplines. Besides optics and photonics, where it appears in the wave scattering theory, it is also useful in quantum particle scattering and astrophysics. In this work, we deal with the OT of the classical time-harmonic electromagnetics; presented below is a brief overview of the most typical scenarios. Those who are interested in the OT in quantum mechanics, can be suggested review [1]. Various more recent theoretical-physics generalizations of the OT have been also published in [2–7].

According to [1], OT has its roots in the 19-th century pioneering works of Sellmeier and Lord Rayleigh, however, was explicitly derived by Mie in 1902 [8]. Still, it had apparently become widely known only since the 1940s, when it was re-discovered by Van de Hulst [9] and, albeit for a short time, bore his name. Originally, it related to the plane-wave scattering from a finite-size object located in the infinite uniform host medium, usually the free space. It links together the sum of the averaged over the period total power taken by the scattered field to infinity and the power lost for absorption (together called the extinction power, or, in the normalized form, extinction cross-section) with the scattered field amplitude in the forward direction. As known, the far-field angular scattering pattern always has a distinctive lobe in the forward direction called

#524420 https://doi.org/10.1364/OE.524420
Journal © 2024 Received 21 Mar 2024; revised 7 Jul 2024; accepted 15 Jul 2024; published 29 Jul 2024

Optics EXPRESS

the shadow lobe. Therefore, the larger or the more lossy the scatterer, the deeper and the longer the shadow behind that scatterer.

Mathematically, derivation of the OT starts from the formulation of the boundary-value problem (BVP) for the set of the time-harmonic Maxwell (in 3-D) or Helmholtz (in 2-D) differential equations plus the boundary conditions at the scatterer surface(s) and the radiation condition at infinity. The OT is obtained by applying the vector (in 3D) or scalar (in 2D) Green's formula to the total field function and its complex conjugate – this is also known as the Complex Poynting Theorem (CPT) [10] – in a limited domain inside a spherical (or circular) layer, external with respect to the scatterer. Then, it is necessary to (i) stretch the outer layer boundary to infinity and use the radiation condition for the field function and (ii) shrink the inner layer boundary to the origin of coordinates and use the boundary conditions. Finally, extraction of the real part of the obtained complex-valued expression yields the sought OT. Therefore, the OT appears as the real part of the CPT and, hence, has the meaning of the power conservation law. It should be noted that it is the presence of the plane-wave term in the total field that is responsible for the appearance, in the OT, of the scattered field amplitude in the forward or shadow direction [11,12].

Thus, the OT is a necessary although not a sufficient condition: every field function, which satisfies the BVP for the Maxwell equations, is destined to satisfy the OT. It has interesting consequences if combined with the Reciprocity Theorem that links together the field generated at the point A by the elementary dipole located at the point B with the reciprocal quantities if A and B are interchanged. If adapted to the plane-wave scattering, this consequence means that the shadow lobe amplitude is invariant with respect to the sign of the incident plane wave propagation direction (although the shape of the whole far-field angular pattern can be drastically different), i.e., the shadow is the same for two opposite illumination directions. Therefore, the extinction power is also invariant of the mentioned direction sign, although the relative contribution of the scattering and the absorption can be different.

If there is no incident plane wave, then the wave-scattering BVP turns into the eigenvalue BVP where the natural-mode frequency must be assumed complex (the real values are not allowed). In such a case, the OT can be applied to the natural-mode field function and its complex conjugate. The resulting expression links the mode Q-factor, defined as the real to twice the imaginary part ratio of the complex eigenfrequency, with the ratio of the power stored in the object as an open resonator to the sum of the powers lost for the radiation and the absorption [13].

The OT has many incarnations depending on the type of the host medium.

If the host medium is not the free space but the space inside a hollow PEC waveguide, then the incident wave cannot be a plane wave – instead, it is one of the natural guided waves of the waveguide. Besides, there is no scattering into the infinite host medium. Assuming that the incident wave carries a unitary power and is defined only in one arm of the waveguide, the OT is relatively easily reduced to $R + T + A = 1$, where R, T and A are the reflectance, transmittance and absorbance, i.e., the corresponding power fractions. In the general case, R and T involve summations over all the natural guided waves that are above cutoff.

If the infinite host medium contains an infinite open waveguide, e.g., it is a lossless layered dielectric medium, then the OT has to contain the terms of both free-space and waveguide nature. For the 2-D case, this derivation was performed in [14] where it was noted that, in that case, the incident field could be not only a plane wave but also a guided wave of the open waveguide. The latter case was in the focus of [15], both in 3-D and 2-D, where the derivation of the OT was linked to the modified radiation condition at infinity, adapted to the existence of the guided natural waves of the open waveguide. Here, the OT has the following normalized form: $R+T+A+S = 1$, where S is the power scattered to the host medium apart from the powers R and T brought to infinity in the backward and forward arms of the open waveguide.

Special case is the plane-wave scattering from infinite periodic scatterers, i.e., the lossless and lossy gratings. Unlike what happens for a finite-size object, here the total powers associated with

Optics EXPRESS

the reflection, transmission and, in the lossy case, absorption are infinite. However, this problem is simply overcome by considering these quantities per single period. Then, the OT takes the same form, $R + T + A = 1$, as in the hollow-waveguide case [16]. This is not surprising as in such scattering problems the additional condition of the quasi-periodicity of the scattered field is present. Thanks to that condition, the whole problem is reduced to a BVP on a single period or, equivalently, in the so-called "Floquet waveguide." However, such an approach cannot be applied when non-periodic infinite structures are involved.

As we have found, an interesting, however, not yet studied case is the plane-wave scattering from an infinite non-periodic lossless or lossy plate-like structure with a 3-D finite-size inhomogeneity.

In a recent paper by the authors [17], dealing with the plane-wave scattering from a resistive plane with a circular hole, it has been demonstrated that, even if an infinite power is absorbed by an infinite holed resistive plane, a change in the size of the circular hole perturbs the density power absorbed, thus suggesting an absorption analysis of the perturbative type. This line of reasoning has been addressed in [18], where, for the same structure, the OT has been formulated by introducing a new easily evaluable parameter for the analysis of the absorption, with a clear physical meaning inferred by the conservation of power principle.

This paper is aimed at presenting the analytical procedure to devise an OT formulation valid for the 3-D scattering from lossless or lossy zero-thickness penetrable resistive plane and thin dielectric plate with finite-size inhomogeneities. Here, we use the term "thin" keeping in mind the model of thinner-than-wavelength dielectric plate, where the thickness shrinks to zero, however, enters the coefficients of the generalized boundary conditions (GBC) [19]. For the sake of simplicity of notation, in Section 2, the OT will be firstly devised for the resistive-plane case, making the generalization to the dielectric plate case, in Section 5, straightforward. Section 3 deals with the derivation of the radiation condition for the diffracted field in the problem at hand, whereas in Section 4, the new OT is formulated. Section 6 shows the numerical results obtained by the analysis, in the optical range, of the plane-wave scattering from a thin dielectric plate with a circular hole sealed with a silver disk. The conclusions are summarized in Section 7. In the paper, we imply the time dependence $e^{j\omega t}$, where ω is the angular frequency.

2. Formulation of the problem

A resistive plane of resistivity R in the free space with a finite-size planar inhomogeneity of resistivity R' is considered (see Fig. 1). A Cartesian coordinate system, (x, y, z), with the z axis orthogonal to the resistive plane and the origin, O, located in the inhomogeneity, and the corresponding cylindrical coordinate system, (ρ, ϕ, z), and spherical coordinate system, (r, θ, ϕ), are introduced.

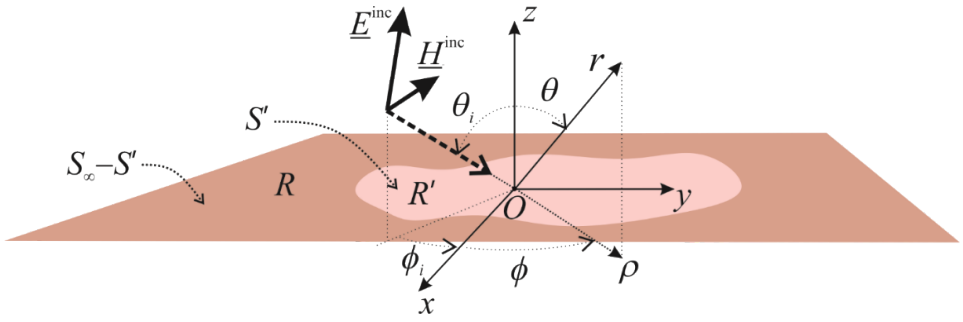

Fig. 1. Geometry of the problem, incident plane wave, and adopted notations.

An incident field, $(\underline{E}^{inc}(\underline{r}),\ \underline{H}^{inc}(\underline{r}))$, where $\underline{r}$ identifies the position of the observation point, impinging onto the structure generates a scattered field. The total field, $(\underline{E}(\underline{r}),\ \underline{H}(\underline{r}))$, given by

Optics EXPRESS

the sum of the incident and scattered fields, can be presented as follows:

$$(\underline{E}(\underline{r}),\ \underline{H}(\underline{r})) = (\underline{E}_0(\underline{r}) + \underline{E}^{\text{diffr}}(\underline{r}),\ \underline{H}_0(\underline{r}) + \underline{H}^{\text{diffr}}(\underline{r})), \tag{1}$$

where $(\underline{E}_0(\underline{r}),\ \underline{H}_0(\underline{r}))$ is the total field of the "background" problem, i.e., the problem involving the homogeneous resistive plane of resistivity R in the free space, and $(\underline{E}^{\text{diffr}}(\underline{r}),\ \underline{H}^{\text{diffr}}(\underline{r}))$ is the diffracted field appearing due to the inhomogeneity. The field of the background problem can be obtained by the separation of variables method and, hence, it is assumed to be known in closed form.

To find the diffracted field, the following BVP appears. The total field must satisfy the time-harmonic Maxwell equations at the points off the plane $z = 0$. At that plane, the two-side resistive boundary conditions [19] are imposed,

$$\underline{E}_t(\rho,\phi,0) = \begin{cases} R\,\underline{J}(\rho,\phi) \text{ for } (\rho,\phi) \in S_\infty - S' \\ R'\underline{J}(\rho,\phi) \text{ for } (\rho,\phi) \in S' \end{cases}, \tag{2a}$$

$$\underline{E}_{0t}(\rho,\phi,0) = R\underline{J}_0(\rho,\phi) \text{ for } (\rho,\phi) \in S_\infty, \tag{2b}$$

where the subscript "t" is used to select the tangential to the plane component of the electric field, S_∞ and S' denote the infinite homogeneous resistive plane and the inhomogeneity region, respectively, and the effective electric surface current densities, $\underline{J}(\rho,\phi)$ and $\underline{J}_0(\rho,\phi)$, are related to the jumps of the tangential to the plane component of the magnetic field with and without the inhomogeneity, respectively, i.e.,

$$\underline{J}(\rho,\phi) = \hat{z} \times (\underline{H}(\rho,\phi,0^+) - \underline{H}(\rho,\phi,0^-)), \tag{3a}$$

$$\underline{J}_0(\rho,\phi) = \hat{z} \times (\underline{H}_0(\rho,\phi,0^+) - \underline{H}_0(\rho,\phi,0^-)). \tag{3b}$$

Additionally, the field must satisfy the local power boundedness condition, which defines the "edge behavior" at the discontinuity, i.e., at the rim of the inhomogeneity region [20]. And, for $r \to +\infty$, the diffracted field must satisfy a radiation condition that eliminates the influx of power from the infinity. Under these conditions, the BVP, where the unknown function is the diffracted field, is uniquely solvable. The radiation condition should be adapted to the "structure of infinity," i.e., account for the presence of the infinite resistive plane. As it will be shown in the next Section, this leads to the asymptotic representation of the diffracted field, at infinity, as a sum of a spherical wave propagating in the $\hat{r}$ direction and, albeit only for a lossless resistive plane, for which $\Re\{R\} = 0$, a cylindrical guided wave propagating in the $\hat{\rho}$ direction [15].

3. Radiation condition for the diffracted field

In the case of a locally perturbed resistive plane, the diffracted field can be always presented as a convolution of the unknown current or its analogue with the Green's function of the uniform resistive plane in the free space. As the convolution is a linear operation, the far-field behavior of the Green's function and of the diffracted field is the same. Therefore, the radiation condition can be established by analyzing the far-zone expression of the Green's function. In the most general form, this expression contains two terms, one bringing the power from infinity to the origin and the other taking the power from the origin to infinity. For uniqueness, only one term of these two must be retained; this must be only the latter term as it agrees with the Principle of Radiation: *no diffracted-field sources at infinity*.

According to this line of reasoning, however, using the Fourier transform (this is also called switching to *the spectral domain*), the diffracted electric and magnetic fields for the problem at

Optics EXPRESS

hand can be expressed in closed form in the spectral domain as functions of the Fourier transform of the effective electric surface current density on the inhomogeneity,

$$\underline{\tilde{J}}(w,\psi) = \frac{1}{4\pi^2}\int_{S'} \underline{J}(\rho,\phi) e^{\mathrm{j}w\rho\cos(\psi-\phi)} dS. \tag{4}$$

Then, the corresponding spatial domain counterparts are retrieved by means of the inverse Fourier transform,

$$\underline{E}^{\mathrm{diffr}}(\underline{r}) = \int_0^{2\pi}\int_C \underline{\tilde{E}}^{\mathrm{diffr}}_{\gtrless}(w,\psi) e^{-\mathrm{j}\underline{k}_{\gtrless}(w,\psi)\cdot\underline{r}} w dw d\psi, \tag{5a}$$

$$\underline{H}^{\mathrm{diffr}}(\underline{r}) = \int_0^{2\pi}\int_C \underline{\tilde{H}}^{\mathrm{diffr}}_{\gtrless}(w,\psi) e^{-\mathrm{j}\underline{k}_{\gtrless}(w,\psi)\cdot\underline{r}} w dw d\psi, \tag{5b}$$

where the subscript ">" ("<") denotes the half-space z>0 (z<0), C is a suitable integration path in the complex plane $w = w_R + \mathrm{j}w_I$ that will be discussed later,

$$\underline{k}_{\gtrless}(w,\psi) = wc_\psi\hat{x} + ws_\psi\hat{y} \mp \mathrm{j}\sqrt{w^2-k_0^2}\hat{z} \tag{6}$$

is the complex wavevector,

$$\underline{\tilde{E}}^{\mathrm{diffr}}_{\gtrless}(w,\psi) = \underline{\underline{\tilde{G}}}_{\gtrless}(w,\psi)\underline{\tilde{J}}(w,\psi), \tag{7a}$$

$$\underline{\tilde{H}}^{\mathrm{diffr}}_{\gtrless}(w,\psi) = \frac{1}{k_0\zeta_0}\underline{k}_{\gtrless}(w,\psi)\times\underline{\tilde{E}}^{\mathrm{diffr}}_{\gtrless}(w,\psi), \tag{7b}$$

are the electric and magnetic fields in the spectral domain, respectively, whereas

$$\underline{\underline{\tilde{G}}}_{\gtrless}(w,\psi) = \frac{R'-R}{\left(-\mathrm{j}\sqrt{w^2-k_0^2}+\frac{2k_0R}{\zeta_0}\right)\left(-\mathrm{j}\sqrt{w^2-k_0^2}+\frac{k_0\zeta_0}{2R}\right)}\bar{\underline{\underline{G}}}_{\gtrless}(w,\psi), \tag{8a}$$

$$\bar{G}_{xx,\gtrless}(w,\psi) = -\mathrm{j}\frac{k_0\zeta_0}{2R}\sqrt{w^2-k_0^2}+k_0^2-w^2c_\psi^2, \tag{8b}$$

$$\bar{G}_{xy,\gtrless}(w,\psi) = \bar{G}_{yx,\gtrless}(w,\psi) = -w^2s_\psi c_\psi, \tag{8c}$$

$$\bar{G}_{yy,\gtrless}(w,\psi) = -\mathrm{j}\frac{k_0\zeta_0}{2R}\sqrt{w^2-k_0^2}+k_0^2-w^2s_\psi^2, \tag{8d}$$

$$\bar{G}_{zx,\gtrless}(w,\psi,z) = \mp wc_\psi\left(-\mathrm{j}\sqrt{w^2-k_0^2}+\frac{k_0\zeta_0}{2R}\right), \tag{8e}$$

$$\bar{G}_{zy,\gtrless}(w,\psi,z) = \mp ws_\psi\left(-\mathrm{j}\sqrt{w^2-k_0^2}+\frac{k_0\zeta_0}{2R}\right), \tag{8f}$$

is part of the 3-D spectral-domain dyadic Green's tensor of the host medium (i.e., the background environment), the components of which are derived using the separation of variables.

Other notations are: $s_t = \sin t$, $c_t = \cos t$, $k_0 = \omega\sqrt{\varepsilon_0\mu_0} = 2\pi/\lambda$ is the free space wavenumber, λ is the free space wavelength, ε_0 and μ_0 denote the dielectric permittivity and the magnetic permeability of the free space, respectively, $\zeta_0 = \sqrt{\mu_0/\varepsilon_0}$ is the free space intrinsic impedance, and $\sqrt{w^2-k_0^2} = \mathrm{j}\sqrt{k_0^2-w^2}$, i.e., the primary sheet of the two-sheeted Riemann surface created by the square-root branch points $\pm k_0$ is chosen.

Optics EXPRESS

Looking at Eqs. from (5) to (8), it is simple to conclude that the integrands in Eq. (5) have two pairs of opposite-sign poles:

$$w_{\mathrm{C}}^{\pm} = \pm\, k_0 \sqrt{1 - \left(\frac{2R}{\zeta_0}\right)^2}, \tag{9a}$$

$$w_{\mathrm{D}}^{\pm} = \pm\, k_0 \sqrt{1 - \left(\frac{\zeta_0}{2R}\right)^2}. \tag{9b}$$

It is worth noting that $w_{\mathrm{C}}^{\pm}$ and $w_{\mathrm{D}}^{\pm}$ are proper poles for $\Im\{R\}>0$ and $\Im\{R\}<0$, respectively, where $\Im\{\cdot\}$ selects the coefficient of the imaginary part of a complex number. Henceforth the symbol $w_P^{\pm}$ will denote two opposite-sign proper poles, meaning that $P = \mathrm{C}$ for $\Im\{R\}>0$ and $P = \mathrm{D}$ for $\Im\{R\}<0$. Moreover, assuming $\Re\{w_P^{+}\}>0$, where $\Re\{\cdot\}$ selects the real part of a complex number, it must be $\Im\{w_P^{+}\}<0$ for $\Re\{R\}>0$, whereas, for $\Re\{R\} = 0$, the poles migrate to the real axis and $w_P^{+}>k_0$. As a result, for $\Re\{R\}>0$, the integration path C detours only around the real-valued square-root branch point k_0 according to the choice of the primary sheet of the corresponding two-sheeted Riemann surface (see Fig. 2(a)), whereas, for $\Re\{R\} = 0$, it has to be additionally deformed in order to detour around the real-valued proper pole w_P^{+} too (see Fig. 2(b)).

By means of Cauchy's integral theorem, Cauchy's residue theorem and Jordan's lemma, it is possible to show that (see Appendix A)

$$\begin{aligned}
\underline{E}^{\mathrm{diffr}}(\underline{r}) = \int_{c_{\phi-\psi}\geq 0} \Bigg[& \int_0^{k_0} \left(\underline{\tilde{E}}_{\gtrless}^{\mathrm{diffr}}(w_R,\psi)\, e^{-\mathrm{j}\underline{k}_{\gtrless}(w_R,\psi)\cdot\underline{r}} - \underline{\tilde{E}}_{-,\gtrless}^{\mathrm{diffr}}(w_R,\psi)\, e^{-\mathrm{j}\underline{k}_{-,\gtrless}(w_R,\psi)\cdot\underline{r}} \right) w_R\, dw_R \\
& - \int_0^{+\infty} \left(\underline{\tilde{E}}_{\gtrless}^{\mathrm{diffr}}(-\mathrm{j}w_I,\psi)\, e^{-\mathrm{j}\underline{k}_{\gtrless}(-\mathrm{j}w_I,\psi)\cdot\underline{r}} + \underline{\tilde{E}}_{-,\gtrless}^{\mathrm{diffr}}(-\mathrm{j}w_I,\psi)\, e^{-\mathrm{j}\underline{k}_{-,\gtrless}(-\mathrm{j}w_I,\psi)\cdot\underline{r}} \right) w_I\, dw_I \\
& - 2\pi\mathrm{j}\underline{\tilde{E}}_{P,\gtrless}^{\mathrm{diffr}}(\psi) e^{-\mathrm{j}\underline{k}_{\gtrless}(w_P^{+},\psi)\cdot\underline{r}} w_P^{+} \Bigg]\, d\psi,
\end{aligned} \tag{10}$$

where the subscript "−" denotes the choice of the secondary sheet of the two-sheeted Riemann surface created by the square-root branch points, i.e., $\sqrt{w^2 - k_0^2} = -\mathrm{j}\sqrt{k_0^2 - w^2}$, and

$$\underline{\tilde{E}}_{P,\gtrless}^{\mathrm{diffr}}(\psi) = \lim_{w\to w_P^{+}} \left(w - w_P^{+}\right) \underline{\tilde{E}}_{\gtrless}^{\mathrm{diffr}}(w,\psi). \tag{11}$$

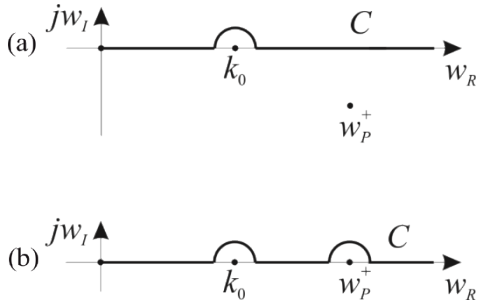

Fig. 2. Inverse Fourier transform integration path C for (a) $\Re\{R\}>0$ and (b) $\Re\{R\} = 0$.

Optics EXPRESS

By means of the stationary phase method, the following asymptotic behavior can be established for the electric field (see Appendix A):

$$\underline{E}^{\mathrm{diffr}}(\underline{r}) \overset{r\to+\infty}{\sim} \underbrace{\frac{e^{-\mathrm{j}k_0 r}}{r}\underline{F}(\theta,\phi)}_{\underline{E}^{\mathrm{diffr}}_{\mathrm{sph}}(\underline{r})} \underbrace{-2\pi\mathrm{j}e^{\mathrm{j}\frac{\pi}{4}}\sqrt{\frac{2\left(w_P^{+2}-k_0^2\right)}{\pi w_P^{+}\rho}}e^{-\mathrm{j}\underline{k}_{\gtrless}\left(w_P^{+},\phi\right)\cdot\underline{r}}\underline{F}_{P,\gtrless}(\phi)}_{\underline{E}^{\mathrm{diffr}}_{\mathrm{cyl}}(\underline{r})}, \tag{12}$$

where

$$\underline{F}(\theta,\phi) = 2\mathrm{j}\pi k_0\left(R'-R\right)\left(\frac{c_\theta\tilde{J}_\rho\left(k_0 s_\theta,\phi\right)}{|c_\theta|+\frac{2R}{\zeta_0}}\hat{\theta}+\frac{\tilde{J}_\phi\left(k_0 s_\theta,\phi\right)}{\frac{1}{|c_\theta|}+\frac{2R}{\zeta_0}}\hat{\phi}\right), \tag{13a}$$

$$\underline{F}_{\mathrm{C},\gtrless}(\phi) = -\mathrm{j}\pi k_0\left(R'-R\right)\tilde{J}_\rho\left(w_{\mathrm{C}}^{+},\phi\right)\left(\frac{2R}{\zeta_0}\hat{\rho}\pm\frac{w_{\mathrm{C}}^{+}}{k_0}\hat{z}\right), \tag{13b}$$

$$\underline{F}_{\mathrm{D},\gtrless}(\phi) = \frac{\mathrm{j}\pi k_0\zeta_0\left(R'-R\right)}{2R}\tilde{J}_\phi\left(w_{\mathrm{D}}^{+},\phi\right)\hat{\phi}. \tag{13c}$$

Further, remembering Eq. (5b) and using Eq. (7b), the asymptotic behavior of the magnetic field can be readily obtained:

$$\underline{H}^{\mathrm{diffr}}(\underline{r}) \overset{r\to+\infty}{\sim} \underline{H}^{\mathrm{diffr}}_{\mathrm{sph}}(\underline{r}) + \underline{H}^{\mathrm{diffr}}_{\mathrm{cyl}}(\underline{r}), \tag{14a}$$

$$\underline{H}^{\mathrm{diffr}}_{\mathrm{sph}}(\underline{r}) = \frac{1}{\zeta_0}\hat{r}\times\underline{E}^{\mathrm{diffr}}_{\mathrm{sph}}(\underline{r}), \tag{14b}$$

$$\underline{H}^{\mathrm{diffr}}_{\mathrm{cyl}}(\underline{r}) = \frac{1}{k_0\zeta_0}\underline{k}_{\gtrless}\left(w_P^{+},\phi\right)\times\underline{E}^{\mathrm{diffr}}_{\mathrm{cyl}}(\underline{r}). \tag{14c}$$

Here, the first field, $(\underline{E}^{\mathrm{diffr}}_{\mathrm{sph}}(\underline{r}), \underline{H}^{\mathrm{diffr}}_{\mathrm{sph}}(\underline{r}))$, is an outgoing electromagnetic spherical wave that satisfies Silver-Muller radiation condition (i.e., TEM wave with respect to $\hat{r}$), whereas the second field, $(\underline{E}^{\mathrm{diffr}}_{\mathrm{cyl}}(\underline{r}), \underline{H}^{\mathrm{diffr}}_{\mathrm{cyl}}(\underline{r}))$, yields one of two outgoing TM and TE polarized with respect to $\hat{\rho}$ and $\hat{z}$ cylindrical guided waves for $P = \mathrm{C}$ and $P = D$, respectively. Such guided waves decay exponentially away from the resistive plane (along the z axis) and algebraically, as $O(\rho^{-1/2})$, along the $\hat{\rho}$ direction. As explained at the end of the previous Section, the asymptotic expressions in Eqs. (12) and (14) can be considered as the analytic form of the radiation condition at infinity, valid for the lossless resistive plane, $\Re\{R\} = 0$, i.e., adapted to the existence of a natural wave guided by such a plane. It should be noted that, if the resistive plane is lossy, i.e., $\Re\{R\}>0$, then the algebraic decay along the $\hat{\rho}$ direction changes to the exponential one. In that case, the second term in Eq. (12) can be safely neglected at infinity, and the radiation condition is reduced to the Silver-Muller condition.

The obtained radiation condition enables us to derive the OT expression, adapted to the presence of the considered infinite resistive plane.

4. Optical theorem

As mentioned in the Introduction section, the tool for devising the OT is the CPT, which is applied to the sphere centered at O, of (finite) radius $\bar{r}$ and volume $\bar{V}$ delimited by the surface $\bar{S}$, containing the inhomogeneity (see Fig. 3). The intersection between the sphere and the plane identifies a zero-thickness disk of radius $\bar{r}$ and surface S. According to the CPT, the real power

Optics EXPRESS

flowing through the surface $\bar{S}$ and the power loss in the volume $\bar{V}$ are related to each other in both the scenarios, with and without the inhomogeneity, by the following relations, respectively:

$$\frac{1}{2}\Re\left\{\oint_{\bar{S}} \underline{E}(\underline{r})\times\underline{H}^{*}(\underline{r})\cdot\hat{r}dS\right\}+\frac{1}{2}\Re\left\{\int_{S}\underline{E}_{t}(\rho,\phi,0)\cdot\underline{J}^{*}(\rho,\phi)dS\right\}=0, \tag{15a}$$

$$\frac{1}{2}\Re\left\{\oint_{\bar{S}} \underline{E}_{0}(\underline{r})\times\underline{H}_{0}^{*}(\underline{r})\cdot\hat{r}dS\right\}+\frac{1}{2}\Re\left\{\int_{S}\underline{E}_{0t}(\rho,\phi,0)\cdot\underline{J}_{0}^{*}(\rho,\phi)dS\right\}=0, \tag{15b}$$

where the star denotes the complex conjugate of a complex number.

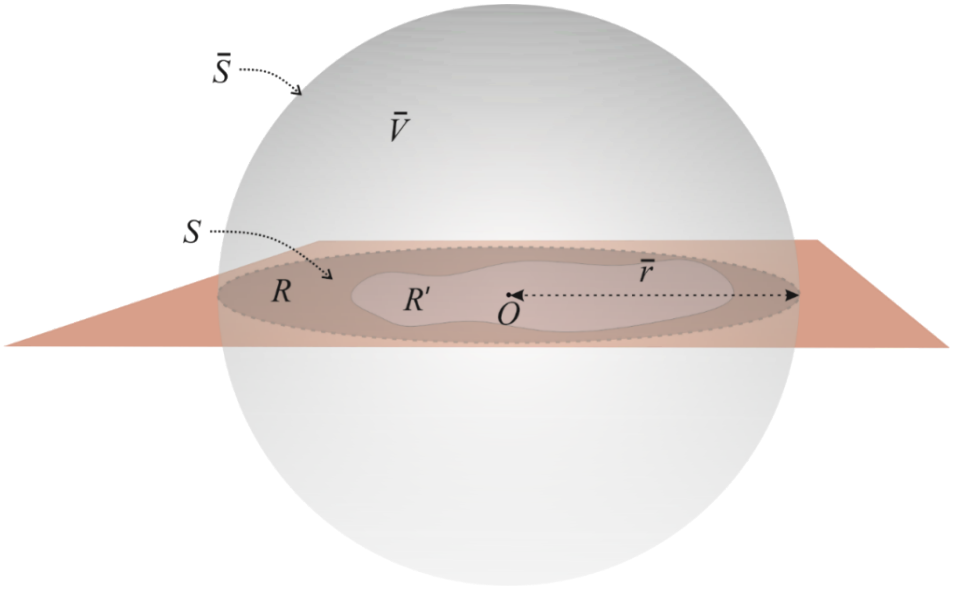

Fig. 3. Geometrical sphere intersecting the scatterer.

By invoking the two-side resistive boundary conditions in Eq. (2), Eqs. (15) can be immediately rewritten as follows:

$$\frac{1}{2}\Re\left\{\oint_{\bar{S}} \underline{E}(\underline{r})\times\underline{H}^{*}(\underline{r})\cdot\hat{r}dS\right\}+\frac{1}{2}\Re\{R\}\int_{S-S'}|\underline{J}(\rho,\phi)|^{2}dS+\frac{1}{2}\Re\{R'\}\int_{S'}|\underline{J}(\rho,\phi)|^{2}dS=0, \tag{16a}$$

$$\frac{1}{2}\Re\left\{\oint_{\bar{S}} \underline{E}_{0}(\underline{r})\times\underline{H}_{0}^{*}(\underline{r})\cdot\hat{r}dS\right\}+\frac{1}{2}\Re\{R\}\int_{S}|\underline{J}_{0}(\rho,\phi)|^{2}dS=0. \tag{16b}$$

Since the OT is expected to involve the far-field behavior, the limit for $\bar{r}\rightarrow+\infty$ of Eqs. (16) has to be performed. However, if $\Re\{R\}>0$, i.e., the resistive plane is made of lossy material, the power loss can increase by enlarging the volume $\bar{V}$, and diverge when $\bar{r}\rightarrow+\infty$ because, independently of the inhomogeneity (that has a finite extent), the surface currents can be asymptotically non-vanishing (as happens, for example, when the incident field is a plane wave). Considering that Eqs. (16) are independent of the sphere radius, it is simple to conclude that

Optics EXPRESS

the limit for $\bar{r} \to +\infty$ of Eqs. (16) can lead to indeterminate forms, i.e., they cannot exist when infinite volumes are involved.

On the other hand, for $\Re\{R\}>0$, remembering Eqs. (1), (3), (12), and (14), it can be observed that

$$\rho(\underline{J}(\rho,\phi)-\underline{J}_0(\rho,\phi))\overset{\rho\to+\infty}{\sim} e^{-\mathrm{j}k_0\rho}\left(F_\theta\left(\frac{\pi}{2}^-,\phi\right)-F_\theta\left(\frac{\pi}{2}^+,\phi\right)\right)=0. \tag{17}$$

As a result, by invoking the triangle inequality, it is simple to state that

$$\left||\underline{J}(\rho,\phi)|^2-|\underline{J}_0(\rho,\phi)|^2\right|\le|\underline{J}(\rho,\phi)-\underline{J}_0(\rho,\phi)|(|\underline{J}(\rho,\phi)|+|\underline{J}_0(\rho,\phi)|)\overset{\rho\to+\infty}{\sim} o(1/\rho). \tag{18}$$

To conclude, the divergence in the power loss can be suppressed and, hence, the indeterminate forms avoided by taking the difference between Eqs. (16a) and (16b) before considering $\bar{r} \to +\infty$, i.e.,

$$\begin{aligned}\frac{1}{2}\Re\left\{\oint_{\bar{S}}\left(\underline{E}_0(\underline{r})\times\underline{H}^{\mathrm{diffr}*}(\underline{r})+\underline{E}^{\mathrm{diffr}}(\underline{r})\times\underline{H}_0^*(\underline{r})\right)\cdot\hat{r}dS\right\}+\frac{1}{2}\Re\left\{\oint_{\bar{S}}\underline{E}^{\mathrm{diffr}}(\underline{r})\times\underline{H}^{\mathrm{diffr}*}(\underline{r})\cdot\hat{r}dS\right\}\\+\frac{1}{2}\Re\{R\}\int_{S-S,}\left(|\underline{J}(\rho,\phi)|^2-\left|\underline{J}_0(\rho,\phi)\right|^2\right)dS+\frac{1}{2}\Re\{R'\}\int_{S'}|\underline{J}(\rho,\phi)|^2dS\\-\frac{1}{2}\Re\{R\}\int_{S'}\left|\underline{J}_0(\rho,\phi)\right|^2dS=0,\end{aligned} \tag{19}$$

where Eq. (1) has been used. As can be simply verified, Eq. (19) is very general including the $\Re\{R\}=0$ case as a special case.

The second integral at the left-hand side of Eq. (19) can be simplified by invoking the radiation condition of the diffracted field. As stated above, when $\bar{r} \to +\infty$, only the spherical wave contributes to the field representation for $\Re\{R\}>0$. Conversely, for $\Re\{R\}=0$, in addition to the spherical wave, the cylindrical wave has to be considered as well. In the latter case, it is simple to show that spherical and cylindrical waves are asymptotically orthogonal in power. Indeed, starting from Eqs. (12) and (14), it is possible to write

$$\begin{aligned}&\frac{1}{2}\oint_{\bar{S}}\underline{E}^{\mathrm{diffr}}_{\mathrm{sph,cyl}}(\underline{r})\times\underline{H}^{\mathrm{diffr}*}_{\mathrm{cyl,sph}}(\underline{r})\cdot\hat{r}dS\\&\qquad=\int_0^{\pi}\int_0^{2\pi}\sqrt{\bar{r}s_\theta}e^{-\bar{r}\left[|c_\theta|\sqrt{w_P^{+2}-k_0^2}\pm\mathrm{j}(k_0-s_\theta w_P^+)\right]}g_P^{\pm}(\theta,\phi)d\theta d\phi,\end{aligned} \tag{20}$$

where $g_P^{\pm}(\theta,\phi)$ are well-behaved functions. Hence, when $\bar{r} \to +\infty$, the integrands decay exponentially for $\theta \neq \pi/2$ and they vanish for $\theta = \pi/2$, i.e., the corresponding integrals asymptotically vanish.

As a result, by means of simple algebraic manipulations, it is possible to conclude that the second integral at the left-hand side of Eq. (19) can be asymptotically written as follows:

$$\begin{aligned}\frac{1}{2}\oint_{\bar{S}}\underline{E}^{\mathrm{diffr}}(\underline{r})\times\underline{H}^{\mathrm{diffr}*}(\underline{r})\cdot\hat{r}dS\overset{\bar{r}\to+\infty}{\sim}\frac{1}{2}\oint_{\bar{S}}\underline{E}^{\mathrm{diffr}}_{\mathrm{sph}}(\underline{r})\times\underline{H}^{\mathrm{diffr}*}_{\mathrm{sph}}(\underline{r})\cdot\hat{r}dS\\+\frac{1}{2}\oint_{\bar{S}}\underline{E}^{\mathrm{diffr}}_{\mathrm{cyl}}(\underline{r})\times\underline{H}^{\mathrm{diffr}*}_{\mathrm{cyl}}(\underline{r})\cdot\hat{r}dS\sim\frac{1}{2\zeta_0}\int_0^{\pi}\int_0^{2\pi}|\underline{F}(\theta,\phi)|^2s_\theta d\theta d\phi\\+\delta_{\Re\{R\},0}\frac{4\pi\zeta_0}{|R|}\int_0^{2\pi}\left|F_{P,p,\gtrless}(\phi)\right|^2d\phi,\end{aligned} \tag{21}$$

where $\delta_{\nu,\mu}$ is the Kronecker delta function, and $p=\rho,\phi$ for $P=\mathrm{C},\ \mathrm{D}$, respectively.

Optics EXPRESS

A suitable choice of the incident field allows us to express the first integral at the left-hand side of Eq. (19) in closed form for $\bar{r} \to +\infty$ by means of the generalization of the procedure proposed by Jones in [21].

If the incident field is a plane wave defined only in the upper half-space (z>0), i.e.,

$$\underline{E}^{\text{inc}}(\underline{r}) = \underline{\bar{E}}^{\text{inc}} e^{-\text{j}\underline{k}_0(\theta_i,\phi_i)\cdot\underline{r}}, \tag{22a}$$

$$\underline{H}^{\text{inc}}(\underline{r}) = \frac{1}{\zeta_0}\hat{k}_0(\theta_i,\phi_i)\times\underline{E}^{\text{inc}}(\underline{r}), \tag{22b}$$

$$\underline{k}_0(\theta,\phi) = k_0\hat{k}_0(\theta_i,\phi_i) = -k_0(s_\theta c_\phi\hat{x} + s_\theta s_\phi\hat{y} + c_\theta\hat{z}), \tag{22c}$$

where $\theta = \theta_i$<$\pi/2$ and $\phi = \phi_i$ identify the incidence direction, then, the plane wave reflected by the homogeneous resistive plane of resistivity R in the upper half-space (z>0) is

$$\underline{E}^{\text{refl}}(\underline{r}) = \underline{\bar{E}}^{\text{refl}} e^{+\text{j}\underline{k}_0(\theta_i,\phi_i\pm\pi)\cdot\underline{r}}, \tag{23a}$$

$$\underline{H}^{\text{refl}}(\underline{r}) = \frac{1}{\zeta_0}\hat{k}_0(\theta_i,\phi_i\pm\pi)\times\underline{E}^{\text{refl}}(\underline{r}), \tag{23b}$$

and the plane wave transmitted by the same plane in the lower half-space (z<0) is

$$\underline{E}^{\text{tr}}(\underline{r}) = \underline{\bar{E}}^{\text{tr}} e^{-\text{j}\underline{k}_0(\pi-\theta_i,\phi_i\pm\pi)\cdot\underline{r}}, \tag{24a}$$

$$\underline{H}^{\text{tr}}(\underline{r}) = \frac{1}{\zeta_0}\hat{k}_0(\pi-\theta_i,\phi_i\pm\pi)\times\underline{E}^{\text{tr}}(\underline{r}), \tag{24b}$$

such that the two-side boundary conditions on the homogeneous resistive plane, i.e., for $(\rho,\phi)\in S_\infty$, are satisfied,

$$\begin{aligned}\underline{E}_t^{\text{inc}}(\rho,\phi,0) + \underline{E}_t^{\text{refl}}(\rho,\phi,0) &= \underline{E}_t^{\text{tr}}(\rho,\phi,0)\\ &= R\hat{z}\times(\underline{H}^{\text{inc}}(\rho,\phi,0) + \underline{H}^{\text{refl}}(\rho,\phi,0) - \underline{H}^{\text{tr}}(\rho,\phi,0)).\end{aligned} \tag{25}$$

Therefore, the total field of the background problem can be written as follows:

$$(\underline{E}_0(\underline{r}),\ \underline{H}_0(\underline{r})) = \begin{cases} (\underline{E}^{\text{inc}}(\underline{r}) + \underline{E}^{\text{refl}}(\underline{r}),\ \underline{H}^{\text{inc}}(\underline{r}) + \underline{H}^{\text{refl}}(\underline{r})) & z>0\\ (\underline{E}^{\text{tr}}(\underline{r}),\ \underline{H}^{\text{tr}}(\underline{r})) & z<0\end{cases}. \tag{26}$$

By means of the stationary phase method and using Eqs. (12), (14), and (26), it can be stated the following asymptotic behavior (see Appendix B):

$$\begin{aligned}&\frac{1}{2}\oint_{\bar{S}}\left(\underline{E}_0(\underline{r})\times\underline{H}^{\text{diffr}*}(\underline{r}) + \underline{E}^{\text{diffr}}(\underline{r})\times\underline{H}_0^*(\underline{r})\right)\cdot\hat{r}dS\\ &\underset{\sim}{\bar{r}\to+\infty}\frac{2\pi}{k_0\zeta_0}\Im\left\{\left[\underline{\bar{E}}^{\text{refl}*}\cdot\underline{F}(\theta_i,\phi_i\pm\pi) + \underline{\bar{E}}^{\text{tr}*}\cdot\underline{F}(\pi-\theta_i,\phi_i\pm\pi)\right]\right\}.\end{aligned} \tag{27}$$

Hence, after normalization of Eq. (19) with the amplitude of the Poynting vector associated with the incident plane wave, $|\underline{\bar{E}}^{\text{inc}}|^2/(2\zeta_0)$, the following generalized version of the OT can be readily established:

$$\sigma_{\text{TSCS}} + \sigma_{\text{ACS}} = -\frac{4\pi}{k_0|\underline{\bar{E}}^{\text{inc}}|^2}\Im\{[\underline{\bar{E}}^{\text{refl}*}\cdot\underline{F}(\theta_i,\phi_i\pm\pi) + \underline{\bar{E}}^{\text{tr}*}\cdot\underline{F}(\pi-\theta_i,\phi_i\pm\pi)]\}. \tag{28}$$

Here, σ_{TSCS} is the total scattering cross-section defined by the diffracted field, expressed as a sum of the spherical wave contribution, σ_{SWCS}, and, only if $\Re\{R\} = 0$, the guided wave

Optics EXPRESS

contribution, σ_{GWCS}, i.e.,

$$\sigma_{\mathrm{TSCS}} = \sigma_{\mathrm{SWCS}} + \sigma_{\mathrm{GWCS}}, \tag{29a}$$

$$\sigma_{\mathrm{SWCS}} = \frac{1}{|\underline{\bar{E}}^{\mathrm{inc}}|^2} \int_0^{\pi} \int_0^{2\pi} |\underline{F}(\theta,\phi)|^2 s_\theta d\theta d\phi, \tag{29b}$$

$$\sigma_{\mathrm{GWCS}} = \delta_{\Re\{R\},0} \frac{8\pi\zeta_0^2}{|R||\underline{\bar{E}}^{\mathrm{inc}}|^2} \int_0^{2\pi} |F_{P,p,\gtrless}(\phi)|^2 d\phi, \tag{29c}$$

and σ_{ACS} is the absorption cross-section defined as the normalized power evaluated on the difference between the density power absorbed in the inhomogeneous and homogeneous cases. The latter quantity can be reviewed as the sum of the variation due to the inhomogeneity of the normalized power absorbed by the resistive plane deprived of the inhomogeneity, $\sigma_{\mathrm{ACS_{ext}}}$, and of the normalized power absorbed by the inhomogeneity itself, $\sigma_{\mathrm{ACS_{int}}}$, i.e.,

$$\sigma_{\mathrm{ACS}} = \sigma_{\mathrm{ACS_{ext}}} + \sigma_{\mathrm{ACS_{int}}}, \tag{30a}$$

$$\sigma_{\mathrm{ACS_{ext}}} = \frac{\zeta_0 \Re\{R\}}{|\underline{\bar{E}}^{\mathrm{inc}}|^2} \left[\int_{S_\infty - S'} (|\underline{J}(\rho,\phi)|^2 - |\underline{J}_0(\rho,\phi)|^2) dS - \int_{S'} |\underline{J}_0(\rho,\phi)|^2 dS \right], \tag{30b}$$

$$\sigma_{\mathrm{ACS_{int}}} = \frac{\zeta_0 \Re\{R'\}}{|\underline{\bar{E}}^{\mathrm{inc}}|^2} \int_{S'} |\underline{J}(\rho,\phi)|^2 dS. \tag{30c}$$

It can be added that the variation of the total power subtracted from the incident plane wave due to the inhomogeneity defines the so-called extinction cross-section, σ_{ECS}, i.e.,

$$\sigma_{\mathrm{ECS}} = \sigma_{\mathrm{TSCS}} + \sigma_{\mathrm{ACS}}. \tag{31}$$

According to Eq. (28), the extinction cross-section is determined by two 3-D "shadow lobes", in the forward direction and in the reflection direction. Moreover, to better clarify the physical meaning of Eq. (31), it is simple to verify that it reduces to the classical OT in [8] and [9] when $R \to \infty$, i.e., when the resistive plane is replaced by the free space.

In the presence of the infinite resistive plane, the combination of the homogeneous plane waves introduced before cannot be used as a background field at the grazing incidence, $\theta = \pi/2$. Still, this configuration offers one more scattering scenario, absent in the case of the free-space scattering. Indeed, the background field can be taken as a plane guided wave propagating along the direction individuated by the angles $\theta = \pi/2$ and $\phi = \phi_i$. In that case, the solution of the background problem can be written as follows:

$$\underline{E}_0(\underline{r}) = \underline{\bar{E}}^{\mathrm{inc}}_{P,\gtrless} e^{-\mathrm{j}\underline{k}_{\gtrless}(w_P^-,\phi_i)\cdot\underline{r}}, \tag{32a}$$

$$\underline{H}_0(\underline{r}) = \frac{1}{k_0\zeta_0} \underline{k}_{\gtrless}\left(w_P^-,\phi_i\right) \times \underline{E}_0(\underline{r}), \tag{32b}$$

where

$$\underline{\bar{E}}^{\mathrm{inc}}_{\mathrm{C},\gtrless} = \bar{E}^{\mathrm{inc}}_{\mathrm{C},\rho_i} \left(\hat{\rho}_i \mp \mathrm{j} \frac{w_{\mathrm{C}}^-}{\sqrt{w_{\mathrm{C}}^{-2} - k_0^2}} \hat{z} \right), \tag{33a}$$

$$\underline{\bar{E}}^{\mathrm{inc}}_{\mathrm{D},\gtrless} = \bar{E}^{\mathrm{inc}}_{\mathrm{D},\phi_i} \hat{\phi}_i. \tag{33b}$$

Of course, since for $\Re\{R\}>0$ the plane guided wave decays exponentially along the propagation direction, only the case of $\Re\{R\} = 0$ can be reasonably considered.

Optics EXPRESS

Once again, by means of the stationary phase method and using Eqs. (12), (14), and (32), the following asymptotic behavior for the first integral at the left hand-side of Eq. (19) can be stated (see Appendix B):

$$\frac{1}{2}\oint_{\bar{S}}\left(\underline{E}_0(\underline{r})\times\underline{H}^{\mathrm{diffr}*}(\underline{r})+\underline{E}^{\mathrm{diffr}}(\underline{r})\times\underline{H}_0^{*}(\underline{r})\right)\cdot\hat{r}dS \underset{\tilde{\sim}}{\bar{r}\to+\infty} \frac{2\pi}{k_0\zeta_0}\Im\left\{\underline{\bar{E}}^{\mathrm{inc}*}_{P,\gtrless}\cdot\underline{F}_{P,\gtrless}(\phi_i\pm\pi)\right\}. \tag{34}$$

To conclude, after normalization of Eq. (19) with the amplitude of the Poynting vector associated with the incident plane guided wave for $z=0$, $\left|\underline{\bar{E}}^{\mathrm{inc}}_{P,\gtrless}\right|^2/(2\zeta_0)$, the OT in Eq. (31) can be readily stated. In such a case,

$$\sigma_{\mathrm{ECS}}=-\frac{4\pi}{k_0\left|\underline{\bar{E}}^{\mathrm{inc}}_{P,\gtrless}\right|^2}\Im\left\{\underline{\bar{E}}^{\mathrm{inc}*}_{P,\gtrless}\cdot\underline{F}_{P,\gtrless}(\phi_i\pm\pi)\right\}, \tag{35}$$

whereas σ_{TSCS} and σ_{ACS} can be obtained starting from Eqs. (29) and (30) by setting $\Re\{R\}=0$ and substituting $\underline{\bar{E}}^{\mathrm{inc}}$ with $\underline{\bar{E}}^{\mathrm{inc}}_{P,\gtrless}$. Note that the right-hand part of (35) has the meaning of the 2-D shadow lobe magnitude in terms of the cylindrical guided wave.

5. Generalization to the dielectric case

The procedure detailed above can be straightforwardly generalized to the scattering from a thin dielectric plate in the free space, which is characterized using the GBC with electric and magnetic resistivities R_{e} and R_{m}, respectively, and perturbed by a local planar inhomogeneity, characterized using the similar GBC with electric and magnetic resistivities R'_{e} and R'_{m}, respectively, and will be omitted in the following for the sake of brevity.

If the incident field is the plane wave defined in Eq. (22), by denoting with σ_{GWCS_q} the guided wave contribution to the total scattering cross-section arising for $\Re\{R_q\}=0$ with $q=\mathrm{e},\mathrm{m}$, it is possible to show that the OT in Eq. (31) can be stated as follows:

$$\sigma_{\mathrm{ECS}}= -\frac{4\pi}{k_0\left|\underline{E}^{\mathrm{inc}}\right|^2}\Im\left\{\left[\underline{\bar{E}}^{\mathrm{refl}*}\cdot\sum_{q=\mathrm{e},\mathrm{m}}\underline{F}_q(\theta_i,\phi_i\pm\pi)+\underline{\bar{E}}^{\mathrm{tr}*}\cdot\sum_{q=\mathrm{e},\mathrm{m}}\underline{F}_q(\pi-\theta_i,\phi_i\pm\pi)\right]\right\}, \tag{36a}$$

$$\sigma_{\mathrm{TSCS}}=\sigma_{\mathrm{SWCS}}+\sum_{q=\mathrm{e},\mathrm{m}}\sigma_{\mathrm{GWCS}_q}, \tag{36b}$$

$$\sigma_{\mathrm{SWCS}}=\frac{1}{\left|\underline{\bar{E}}^{\mathrm{inc}}\right|^2}\int_0^{\pi}\int_0^{2\pi}\left|\sum_{q=\mathrm{e},\mathrm{m}}\underline{F}_q(\theta,\phi)\right|^2 s_\theta d\theta d\phi, \tag{36c}$$

$$\sigma_{\mathrm{GWCS}_q}=\delta_{\Re\{R_q\},0}\frac{8\pi\zeta_0^2}{|R_q|\left|\underline{\bar{E}}^{\mathrm{inc}}\right|^2}\int_0^{2\pi}|F_{q,P,p,\gtrless}(\phi)|^2 d\phi, \tag{36d}$$

$$\sigma_{\mathrm{ACS}}=\sigma_{\mathrm{ACS}_{\mathrm{ext}}}+\sigma_{\mathrm{ACS}_{\mathrm{int}}}, \tag{36e}$$

$$\sigma_{\mathrm{ACS}_{\mathrm{ext}}}= \sum_{q=\mathrm{e},\mathrm{m}}\frac{\zeta_0\Re\{R_q\}}{\left|\underline{E}^{\mathrm{inc}}\right|^2}\left[\int_{S_\infty-S'}\left(\left|\underline{J}_q(\rho,\phi)\right|^2-|\underline{J}_{q0}(\rho,\phi)|^2\right)dS-\int_{S'}\left|\underline{J}_{q0}(\rho,\phi)\right|^2 dS\right], \tag{36f}$$

Optics EXPRESS

$$\sigma_{\mathrm{ACS_{int}}} = \sum_{q=\mathrm{e,m}} \frac{\zeta_0 \Re\{R'_q\}}{\left|\underline{E}^{\mathrm{inc}}\right|^2} \int_{S'} |\underline{J}_q(\rho,\phi)|^2 dS, \tag{36g}$$

where

$$\underline{F}_{\mathrm{e}}(\theta,\phi) = \mathrm{j}2\pi k_0 (R'_{\mathrm{e}} - R_{\mathrm{e}}) \left(\frac{c_\theta \tilde{J}_{\mathrm{e},\rho}(k_0 s_\theta,\phi)}{|c_\theta| + \frac{2R_{\mathrm{e}}}{\zeta_0}} \hat{\theta} + \frac{\tilde{J}_{\mathrm{e},\phi}(k_0 s_\theta,\phi)}{\frac{1}{|c_\theta|} + \frac{2R_{\mathrm{e}}}{\zeta_0}} \hat{\phi} \right), \tag{37a}$$

$$\underline{F}_{\mathrm{m}}(\theta,\phi) = \mathrm{j}2\pi k_0 \zeta_0 (R'_{\mathrm{m}} - R_{\mathrm{m}}) \left(\frac{\tilde{J}_{\mathrm{m},\phi}(k_0 s_\theta,\phi)}{\frac{1}{|c_\theta|} + 2\zeta_0 R_{\mathrm{m}}} \hat{\theta} - \frac{c_\theta \tilde{J}_{\mathrm{m},\rho}(k_0 s_\theta,\phi)}{|c_\theta| + 2\zeta_0 R_{\mathrm{m}}} \hat{\phi} \right), \tag{37b}$$

$$\underline{F}_{\mathrm{e,C},\gtrless}(\phi,z) = -\mathrm{j}\pi k_0 \left(R'_{\mathrm{e}} - R_{\mathrm{e}}\right) \tilde{J}_{\mathrm{e},\rho}\left(w^{+}_{\mathrm{e,C}},\phi\right) \left(\frac{2R_{\mathrm{e}}}{\zeta_0} \hat{\rho} \pm \frac{w^{+}_{\mathrm{e,C}}}{k_0} \hat{z} \right), \tag{37c}$$

$$\underline{F}_{\mathrm{e,D},\gtrless}(\phi,z) = \frac{\mathrm{j}\pi k_0 \zeta_0 \left(R'_{\mathrm{e}} - R_{\mathrm{e}}\right)}{2R_{\mathrm{e}}} \tilde{J}_{\mathrm{e},\phi}\left(w^{+}_{\mathrm{e,D}},\phi\right) \hat{\phi}, \tag{37d}$$

$$\underline{F}_{\mathrm{m,C},\gtrless}(\phi,z) = \mp \frac{\mathrm{j}\pi k_0 \zeta_0 \left(R'_{\mathrm{m}} - R_{\mathrm{m}}\right)}{2} \tilde{J}_{\mathrm{m},\rho}\left(w^{+}_{\mathrm{m,C}},\phi\right) \hat{\phi}, \tag{37e}$$

$$\underline{F}_{\mathrm{m,D},\gtrless}(\phi,z) = -\frac{\mathrm{j}\pi k_0 \left(R'_{\mathrm{m}} - R_{\mathrm{m}}\right)}{2R_{\mathrm{m}}} \tilde{J}_{\mathrm{m},\phi}\left(w^{+}_{\mathrm{m,D}},\phi\right) \left(\pm \frac{1}{2R_{\mathrm{m}}\zeta_0} \hat{\rho} + \frac{w^{+}_{\mathrm{m,D}}}{k_0} \hat{z} \right), \tag{37f}$$

the effective electric and magnetic surface current densities, $\underline{J}_{\mathrm{e}}(\rho,\phi), \underline{J}_{\mathrm{e0}}(\rho,\phi)$ and $\underline{J}_{\mathrm{m}}(\rho,\phi)$, $\underline{J}_{\mathrm{m0}}(\rho,\phi)$, are related to the jumps across the plane of the tangential to the plane component of the magnetic and electric fields with and without the inhomogeneity, respectively [19], $\tilde{J}_q(w,\psi)$ is the Fourier transform of the effective electric/magnetic surface current density on the inhomogeneity,

$$w^{\pm}_{\mathrm{e,C}} = \pm k_0 \sqrt{1 - \left(\frac{2R_{\mathrm{e}}}{\zeta_0}\right)^2}, \tag{38a}$$

$$w^{\pm}_{\mathrm{e,D}} = \pm k_0 \sqrt{1 - \left(\frac{\zeta_0}{2R_{\mathrm{e}}}\right)^2}, \tag{38b}$$

$$w^{\pm}_{\mathrm{m,C}} = \pm k_0 \sqrt{1 - (2\zeta_0 R_{\mathrm{m}})^2}, \tag{38c}$$

$$w^{\pm}_{\mathrm{m,D}} = \pm k_0 \sqrt{1 - \left(\frac{1}{2\zeta_0 R_{\mathrm{m}}}\right)^2}, \tag{38d}$$

are the poles of the Green's function of the background problem, and $w^{\pm}_{q,\mathrm{C}}$ and $w^{\pm}_{q,\mathrm{D}}$ are proper poles for $\Im\{R_q\}>0$ and $\Im\{R_q\}<0$, respectively. For the sake of completeness, it is worth observing that, according to the GBC, $\Re\{R_{\mathrm{e}}\} = 0 \Leftrightarrow \Re\{R_{\mathrm{m}}\} = 0$.

On the other hand, assuming that the incident field is the guided plane wave defined in Eq. (32), the OT in Eq. (31) can be readily stated providing that

$$\sigma_{\mathrm{ECS}} = -\frac{4\pi}{k_0 \left|\underline{\tilde{E}}^{\mathrm{inc}}_{P,\gtrless}\right|^2} \Im \left\{ \underline{\tilde{E}}^{\mathrm{inc}*}_{P,\gtrless} \cdot \sum_{q=\mathrm{e,m}} \underline{F}_{q,P,\gtrless}\left(\phi_i \pm \pi\right) \right\}, \tag{39}$$

whereas σ_{TSCS} and σ_{ACS} can be obtained starting from Eq. (36) by setting $\Re\{R\} = 0$ and substituting $\underline{\tilde{E}}^{\mathrm{inc}}$ with $\underline{\tilde{E}}^{\mathrm{inc}}_{P,\gtrless}$.

Optics EXPRESS

6. Numerical results

In this Section, the theory developed in the previous Sections is applied to the case of a silver disk-sealed circular hole in a thin dielectric plate with, just as an example, the same thickness (in fact, different thicknesses of the disk and the plate can be taken provided that each of them is much smaller than the free-space wavelength). In such a case, the scattering problem can be cast to integral equations and solved numerically, with mathematically guaranteed convergence, by the regularizing Helmholtz-Galerkin technique developed by the authors earlier [17,22]. Here, we use the explicit expressions for the electric and magnetic resistivities obtained by applying Karlsson's compensation [23] to the well-established expressions of [19]. Note that the mentioned technique is full-wave and meshless one; it has been extensively verified in [17,22] including comparison with commercial software.

The analysis will be carried out in the visible range, where the silver relative dielectric permittivity, ε_r', is a complex-valued function of the wavelength, with the real part varying from small positive values in UV to large negative ones at the rest of the range. To this purpose, the experimental data presented in [24], together with the Akima spline interpolation algorithm, will be used to obtain the relative dielectric permittivity at any wavelength of interest. As known [25], the infinite flat layer of a noble metal in the free space supports the propagation of two hybrid 2-D surface plasmon guided waves, symmetric or "long-range" (HSP^{+}) and anti-symmetric or "short-range" (HSP^{-}) ones. The latter wave has a remarkable property: the thinner the layer, the larger the propagation constant, i.e., the shorter the length of that wave and the stronger the field confinement. In contrast, the former wave has the propagation constant very close to the free-space wavenumber. The same two HSP guided waves can also propagate on a metal layer as cylindrical 3-D waves, with the same propagation constants as the 2-D waves.

Moreover, on a finite thin metallic object – the silver disk in our case – the surface plasmon guided waves are able to reflect from the object rim and form standing waves. Therefore, the metal disk can be viewed as Fabry–Perot-like circular resonator, which possesses the corresponding natural modes. Here, the reasonable Q-factor modes originate only from the "short-range" plasmon guided wave HSP^{-} because its field is well compressed to the disk.

In the following, these disk plasmon modes will be denoted as P_{mn}, where the subscripts m and n account for the azimuthal and radial variations, respectively. The resonances on these modes are simply individuated by the peaks of the scattering and absorption characteristics defined in Eq. (36). For the sake of simplicity of notation, henceforth, the following acronyms will be introduced:

- $\mathrm{ACS}_{\mathrm{ext}}$: absorption cross-section associated with the variation due to the inhomogeneity of the power absorbed by the thin dielectric plate deprived of the inhomogeneity;
- $\mathrm{ACS}_{\mathrm{int}}$: absorption cross-section associated with the power absorbed by the inhomogeneity;
- GWCS_q with $q = \mathrm{e}, \mathrm{m}$: guided wave contribution to the total scattering cross-section arising for $\Re\{R_q\} = 0$;
- SWCS: spherical wave contribution to the total scattering cross-section.

As the first example, shown in Fig. 4, comparisons are provided between a silver disk in a homogeneous lossless medium (case 1) and a silver disk in a lossless thin dielectric plate immersed in vacuum (case 2) for the wavelength varying in the visible range. The medium in case 1 and the plate in case 2 have the same relative dielectric permittivity, which assumes 3 different values, $\varepsilon_r = 1,\ 2.25,\ 12$. Moreover, the silver disk radius is $a = 50$ nm, the disk and dielectric plate thickness is $\tau = 20$ nm, and the plane wave normally impinges onto the scatterers ($\theta_i = 0°$), i.e., the incident field is homogeneous on the scatterer surface, thus exciting only the Fourier harmonics of order ± 1. This phenomenon can be simply explained observing that the azimuthal

Optics EXPRESS

harmonics are independent of each other due to the azimuthal symmetry of the problem at hand, and that the only non-vanishing Fourier harmonics contribution of an in-plane homogeneous field are the ones of order ±1. Of course, for $\varepsilon_r = 1$, we have exactly the same structure in both the cases: a silver disk in vacuum. Hence, as expected, the corresponding behavior of SWCS and $\mathrm{ACS_{int}}$ is exactly the same (see the first subpanel of Figs. 4(a) and 4(b)). Moreover, no guided waves can be excited without a dielectric plate, hence, $\mathrm{GWCS_e}$ and $\mathrm{GWCS_m}$ vanish in case 2. A maximum can be clearly observed associated with the plasmon mode resonance P_{11} of the silver disk, which will be discussed later. By increasing the relative dielectric permittivity, this resonance up-shifts in both cases (see the second and third subpanels of Figs. 4(a) and 4(b)). However, in case 2, the shift is smaller and, despite what happens in case 1, the peaks become wider, thus implying a poorer confinement of the field, i.e., a lower value of the associated quality factor. Moreover, guided waves are excited in the dielectric plate. The amplitude of $\mathrm{GWCS_e}$ increases by increasing the relative dielectric permittivity of the plate, becoming even larger than $\mathrm{ACS_{int}}$ and SWCS for $\varepsilon_r = 12$. Since $\mathrm{GWCS_m}$ cannot be appreciated in Fig. 4(b), a zoom in logscale of both $\mathrm{GWCS_e}$ and $\mathrm{GWCS_m}$ is provided in Figs. 4(c) and 4(d), respectively. Such figures confirm that $\mathrm{GWCS_m} \ll \mathrm{GWCS_e}$. This result can be explained by observing the subsequent figures. In the frequency range of interest, Fig. 4(e) shows the purely imaginary electric and magnetic resistivities of the dielectric plate, R_e and R_m, normalized to the intrinsic impedance of vacuum, whereas, the variation with respect to the free space wavenumber of the (real) propagation constants of the associated guided waves, $w^+_{\mathrm{e,D}}$ and $w^+_{\mathrm{m,D}}$, are plotted in Fig. 4(f). As can be clearly seen, the larger values of the normalized magnetic resistivity are reflected in a propagation constant of the corresponding guided wave very close to the free space wavenumber, and, hence, in a poor confinement of the guided wave. On the contrary, the larger values of $\mathrm{GWCS_e}$, comparable with $\mathrm{ACS_{int}}$ and SWCS, are associated with a stronger confinement of the wave caused by smaller values of the normalized electric resistivity and, consequently, larger with respect to the free space wavenumber values of the associated propagation constant.

The behavior of $\mathrm{GWCS_e}$ for $\varepsilon_r = 2.25$ in Fig. 4(c) exhibits a minimum at the wavelength 315.7 nm (marked in the figure). Moreover, minima at about the same wavelength can be appreciated even observing the behavior of SWCS and $\mathrm{GWCS_m}$ in Figs. 4(b) and 4(d), respectively, and the behavior of SWCS, $\mathrm{GWCS_e}$, and, for a lossy dielectric plate, of $\mathrm{ACS_{ext}}$ in the subsequent figures. These minima can be explained by observing that the wavelength 315.7 nm is very close to the wavelength 316.2 nm at which $|\varepsilon'_r - 2.25|$, where $\varepsilon'_r = 0.74 - \mathrm{j}0.84$, assumes the minimum value, of about 1.7, in the visible range. Hence, at this wavelength, the diffracted field reduces significantly because the discontinuity between the silver disk and the dielectric plate is softened, thus resulting in a sort of "invisibility" of the silver disk in the background environment, i.e., the inhomogeneous structure behaves almost like a homogeneous one. It is interesting to note that, at the same wavelength, $\mathrm{ACS_{int}}$ does not show that kind of minimum because the silver disk losses cannot be neglected due to the significant imaginary part of ε'_r. To conclude, it is worth observing that such an effect cannot be appreciated for $\varepsilon_r = 12$ because the minimum value of $|\varepsilon'_r - 12|$ in the visible range is too large (about 6 time larger than $|\varepsilon'_r - 2.25|$).

In Figs. from 5 to 8, the scattering from a silver disk in a lossless thin dielectric plate, with a relative dielectric permittivity $\varepsilon_r = 2.25$, and in a lossy dielectric plate with a relative dielectric permittivity $\varepsilon_r = 2.25(1 - \mathrm{j}10^{-2})$ is analyzed for varying values of the wavelength in the visible range. The reason for choosing such a small imaginary part of the relative permittivity of the dielectric plate is the need of clearly showing the relation between the power associated with the guided waves arising for $\varepsilon_r = 2.25$ and the variation due to the inhomogeneity of the power absorbed by the dielectric plate deprived of the inhomogeneity region for $\varepsilon_r = 2.25(1 - \mathrm{j}10^{-2})$, being the power associated with the spherical wave and the power absorbed by the silver disk very close to each other in the two cases examined.

Optics EXPRESS

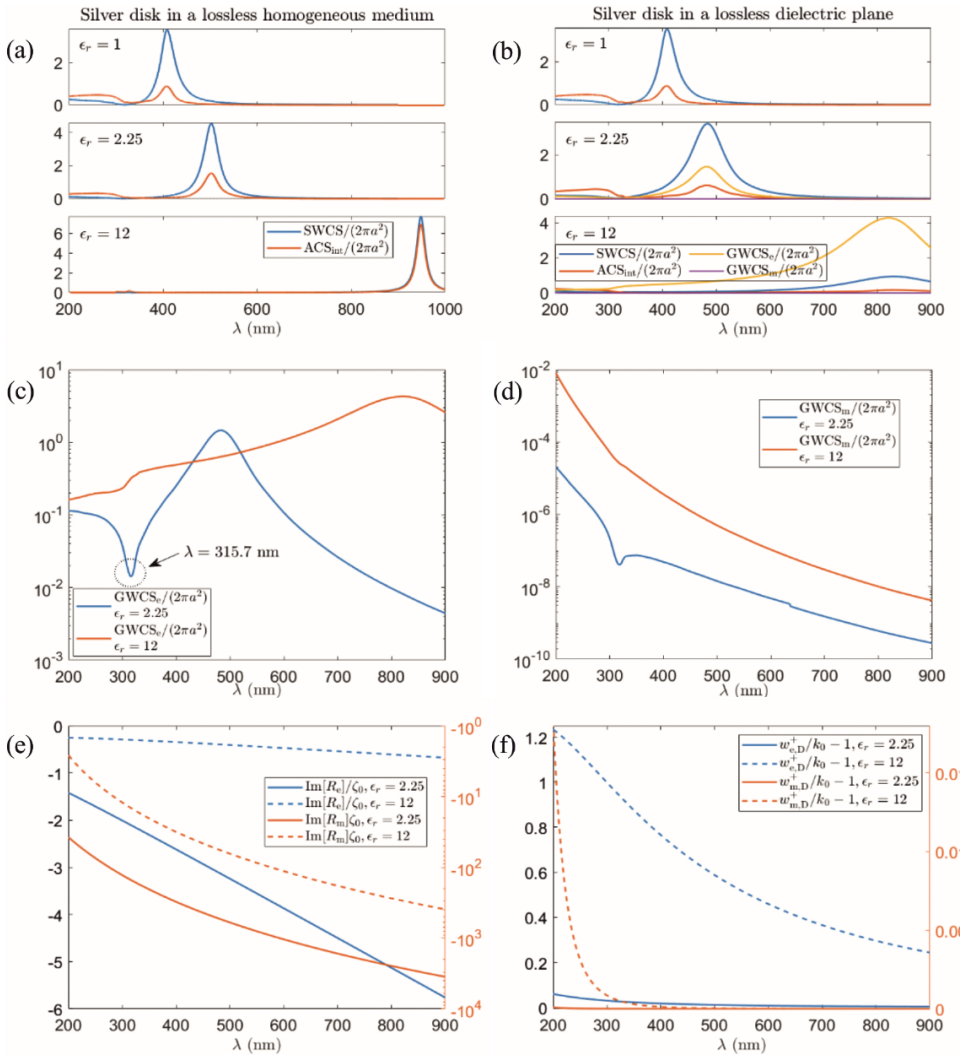

Fig. 4. Normal incidence of the plane wave onto a silver disk of radius $a = 50$ nm in (a) a lossless homogeneous medium, and (b), (c) and (d) a lossless dielectric plate, for structure thickness $\tau = 20$ nm and relative dielectric permittivity $\varepsilon_r = 1, 2.25, 12$. Behavior in the optical range of: (a) SWCS and $\mathrm{ACS_{int}}$ for the homogeneous medium case; (b) SWCS, $\mathrm{ACS_{int}}$, $\mathrm{GWCS_e}$, $\mathrm{GWCS_m}$, (c) $\mathrm{GWCS_e}$, (d) $\mathrm{GWCS_m}$ for the dielectric plate case. (e) Resistivities and (f) propagation constants of the guided waves in a lossless dielectric plate of thickness $\tau = 20$ nm and relative dielectric permittivity $\varepsilon_r = 2.25, 12$.

In Fig. 5, the silver disk radius is $a = 50$ nm, 3 values of the structure thickness are $\tau = 5, 10, 20$ nm, and normal incidence of the plane wave is considered. The plots in Figs. 5(a) and 5(b) show that the resonance wavelength up-shifts by decreasing the thickness of the structure. This is because of the mentioned property of the hybrid plasmon guided wave HSP^-, which is responsible for the disk plasmon modes: the thinner the metal layer, the shorter the wavelength of that wave [25]. Moreover, the peaks get narrower for the smaller thickness, i.e., the mode Q-factors get higher. To conclude, higher order resonances of the kind P_{1n} are excited for smaller values of the thickness as evidenced by the new peaks marked in Fig. 5(d).

Optics EXPRESS

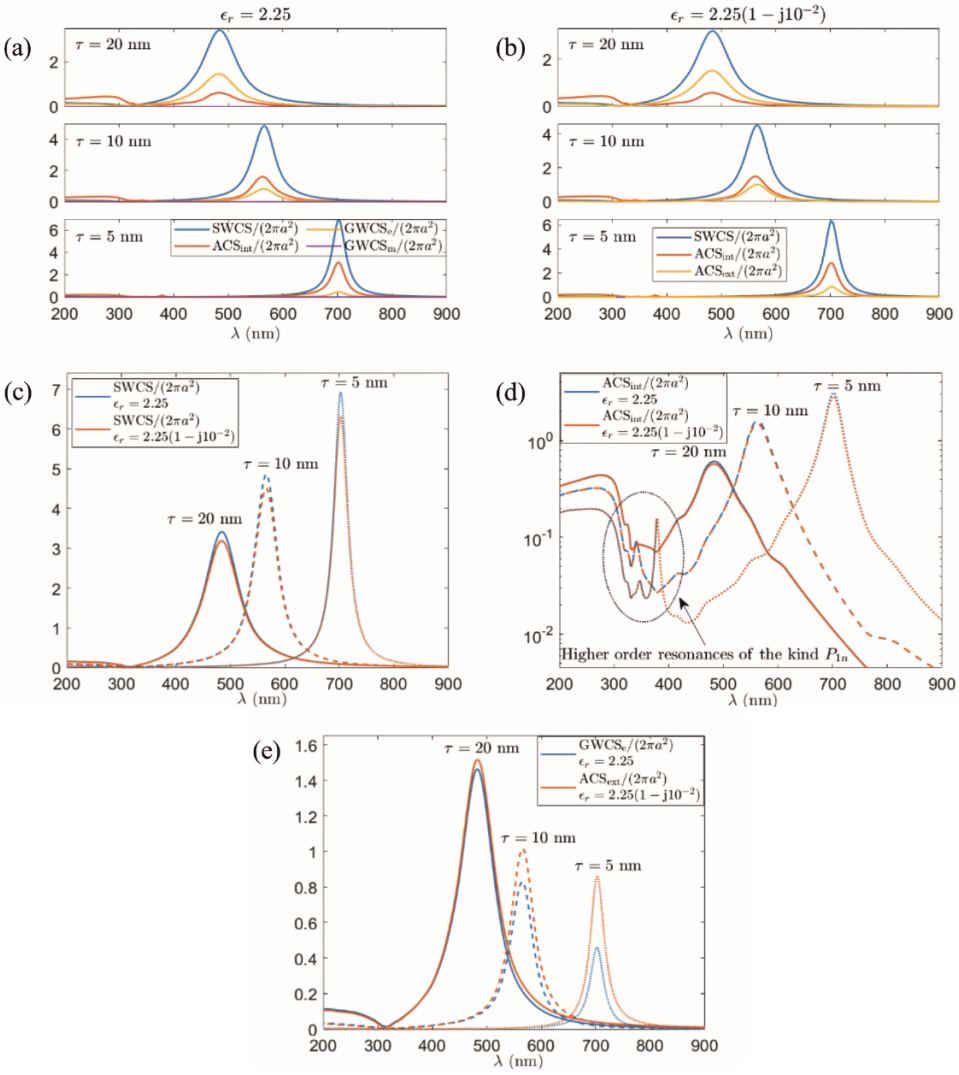

Fig. 5. Normal incidence of the plane wave onto a silver disk of radius $a = 50$ nm in a lossless/lossy dielectric plate of the relative permittivity $\varepsilon_r = 2.25/\varepsilon_r = 2.25(1 - j10^{-2})$ for structure thickness $\tau = 5,\ 10,\ 20$ nm. Behavior in the optical range of: (a) SWCS, ACS_{int}, $GWCS_e$, and $GWCS_m$ for the lossless case; (b) SWCS, ACS_{int}, and ACS_{ext} for the lossy case; (c) SWCS and (d) ACS_{int} for the lossless case and the lossy case, respectively; (e) $GWCS_e$ for the lossless case and ACS_{ext} for the lossy case.

Optics EXPRESS

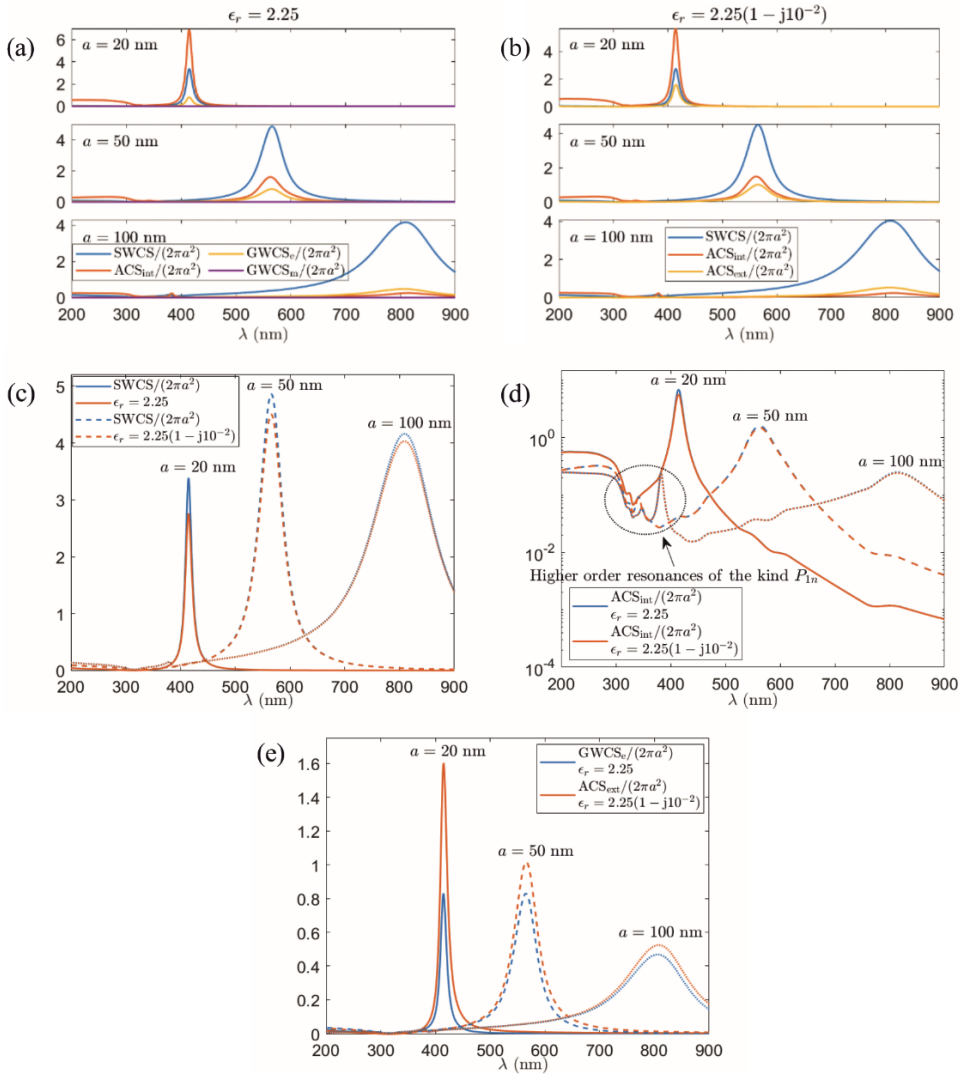

Fig. 6. Normal incidence of the plane wave onto a silver disk in a lossless/lossy dielectric plate of relative permittivity $\varepsilon_r = 2.25/\varepsilon_r = 2.25(1 - j10^{-2})$ for structure thickness $\tau = 10$ nm and disk radius $a = 20,\ 50,\ 100$ nm. Behavior in the optical range of: (a) SWCS, ACS_{int}, $GWCS_e$, and $GWCS_m$ for the lossless case; (b) SWCS, ACS_{int}, and ACS_{ext} for the lossy case; (c) SWCS and (d) ACS_{int} for the lossless case and the lossy case, respectively; (e) $GWCS_e$ for the lossless case and ACS_{ext} for the lossy case.

Direct comparisons between SWCS and ACS_{int} for the lossless and the lossy cases are provided in Figs. 5(c) and 5(d). A small discrepancy, which increases by decreasing the thickness, can be observed on SWCS, whereas ACS_{int} does not show appreciable variations. On the other hand, since the guided waves cannot carry the power to infinity in the lossy case, $GWCS_e$ and $GWCS_m$ are replaced by ACS_{ext} in that case. As stated before, $GWCS_m$ can be neglected (henceforth this assumption will be implicitly done), hence, just comparisons between $GWCS_e$ in the lossless case and ACS_{ext} in the lossy case are shown in Fig. 5(e). Even in such a case, a similar behavior can be appreciated with discrepancies that increase by decreasing the thickness.

Optics EXPRESS

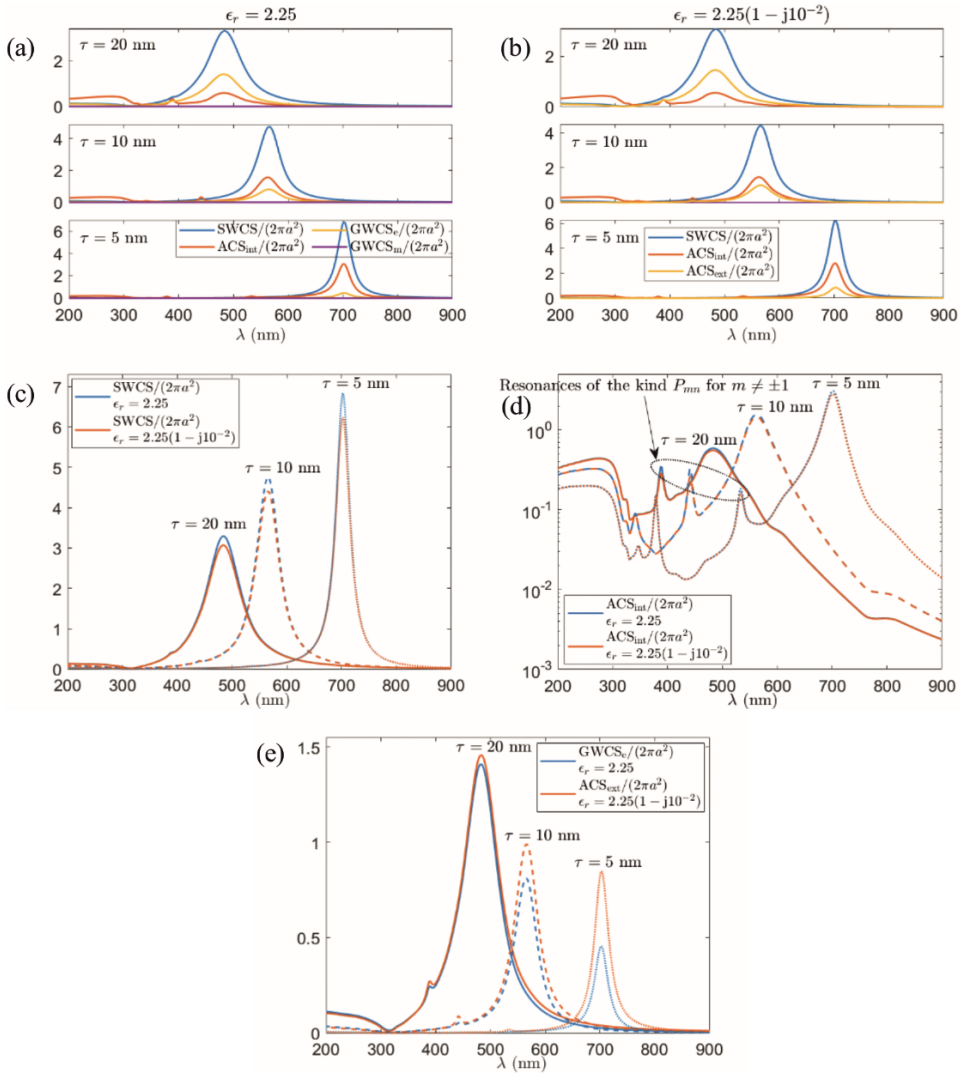

Fig. 7. TE incidence of the plane wave, with incidence angles $\theta_i = 30°$ and $\phi_i = 0°$, onto a silver disk of radius $a = 50$ nm in a lossless/lossy dielectric plate of relative permittivity $\varepsilon_r = 2.25/\varepsilon_r = 2.25(1 - j10^{-2})$ for structure thickness $\tau = 5,\ 10,\ 20$ nm. Behavior in the optical range of: (a) SWCS, ACS_{int}, $GWCS_e$, and $GWCS_m$ for the lossless case; (b) SWCS, ACS_{int}, and ACS_{ext} for the lossy case; (c) SWCS and (d) ACS_{int} for the lossless case and the lossy case, respectively; (e) $GWCS_e$ for the lossless case and ACS_{ext} for the lossy case.

Figure 6 shows the results of the analysis for 3 values of the silver disk radius, $a = 20, 50, 100$ nm, structure thickness $\tau = 10$ nm, and normal incidence of the plane wave. Figures 6(a) and 6(b) clearly show that the resonance wavelength up-shifts by increasing the disk radius. Moreover, the peaks are wider the larger the radius is. As expected, new peaks can be observed for larger size of the disk, i.e., for increasing values of the disk radius, associated with higher order resonances on the modes P_{1n} (see the peaks marked in Fig. 6(d)). Direct comparisons between SWCS and ACS_{int} for the lossless and the lossy cases are provided in Figs. 6(c) and 6(d). Once again, small discrepancies, which decrease by increasing the disk radius, can be observed on SWCS, whereas ACS_{int} does not show appreciable variations. Comparisons between $GWCS_e$ in the lossless case

Optics EXPRESS

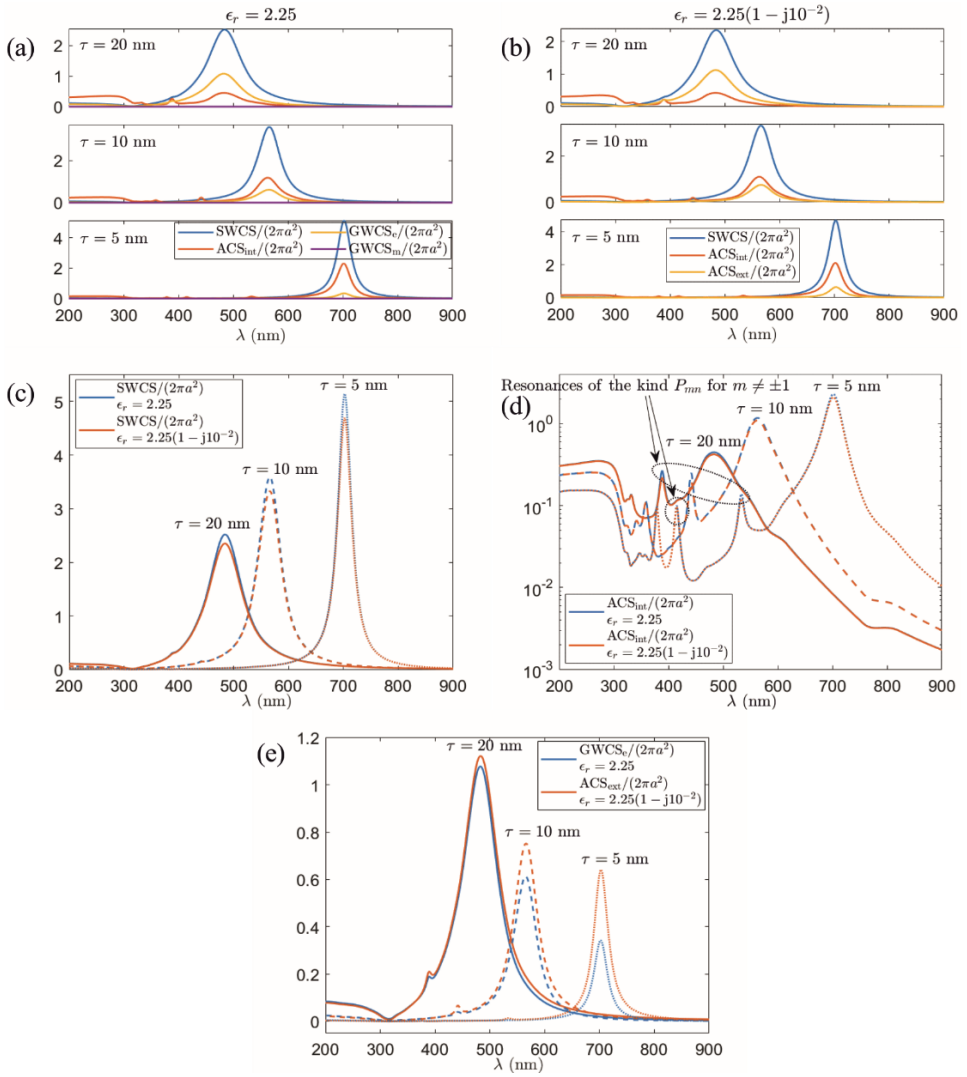

Fig. 8. TM incidence of the plane wave, with incidence angles $\theta_i = 30°$ and $\phi_i = 0°$, onto a silver disk of radius $a = 50$ nm in a lossless/lossy dielectric plate of relative permittivity $\varepsilon_r = 2.25/\varepsilon_r = 2.25(1 - j10^{-2})$ for structure thickness $\tau = 5,\ 10,\ 20$ nm. Behavior in the optical range of: (a) SWCS, ACS$_{int}$, GWCS$_e$, and GWCS$_m$ for the lossless case; (b) SWCS, ACS$_{int}$, and ACS$_{ext}$ for the lossy case; (c) SWCS and (d) ACS$_{int}$ for the lossless case and the lossy case, respectively; (e) GWCS$_e$ for the lossless case and ACS$_{ext}$ for the lossy case.

and ACS$_{ext}$ in the lossy case are provided in Fig. 6(e) showing discrepancies that decrease by increasing the disk radius.

In Figs. 7 and 8, the cases with silver disk radius $a = 50$ nm, 3 values of the structure thickness, $\tau = 5, 10, 20$ nm, and, respectively, oblique TE and TM incidences of the plane wave with $\theta_i = 30°$ and $\phi_i = 0°$ are considered. All the considerations done with reference to the behavior in Fig. 5 can be immediately extended to these cases. As a matter of fact, the resonance wavelength up-shifts by decreasing the structure thickness, the peaks get narrower for the smaller thickness, and higher order resonances on the modes P_{1n} are excited. However, since here all the cylindrical harmonics are present, apart from the peaks observed for the normal incidence, new peaks arise

Optics EXPRESS

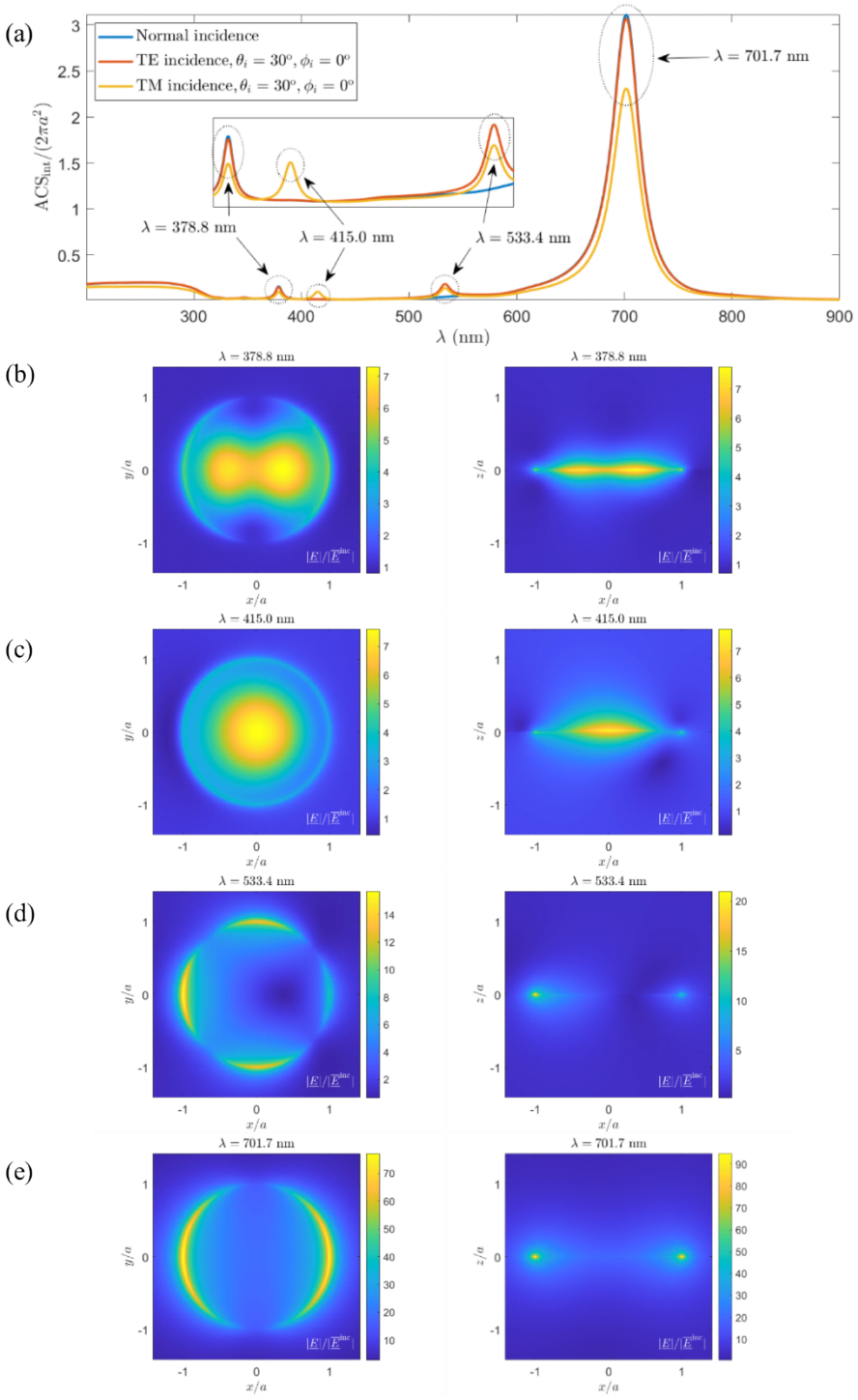

Fig. 9. Plane-wave scattering from a silver disk of radius $a = 50$ nm in a lossless dielectric plate of relative permittivity $\varepsilon_r = 2.25$ for structure thickness $\tau = 5$ nm. (a) Behavior in the optical range of $\mathrm{ACS_{int}}$ for normal incidence, and for TE and TM incidences with incidence angles $\theta_i = 30°$ and $\phi_i = 0°$. Electric field behavior at the resonance wavelengths marked in (a) for oblique TM incidence of the plane wave with $\theta_i = 30°$ and $\phi_i = 0°$: (b) $\lambda = 378.8$ nm; (c) $\lambda = 415.0$ nm; (d) $\lambda = 533.4$ nm; (e) $\lambda = 701.7$ nm.

Optics EXPRESS

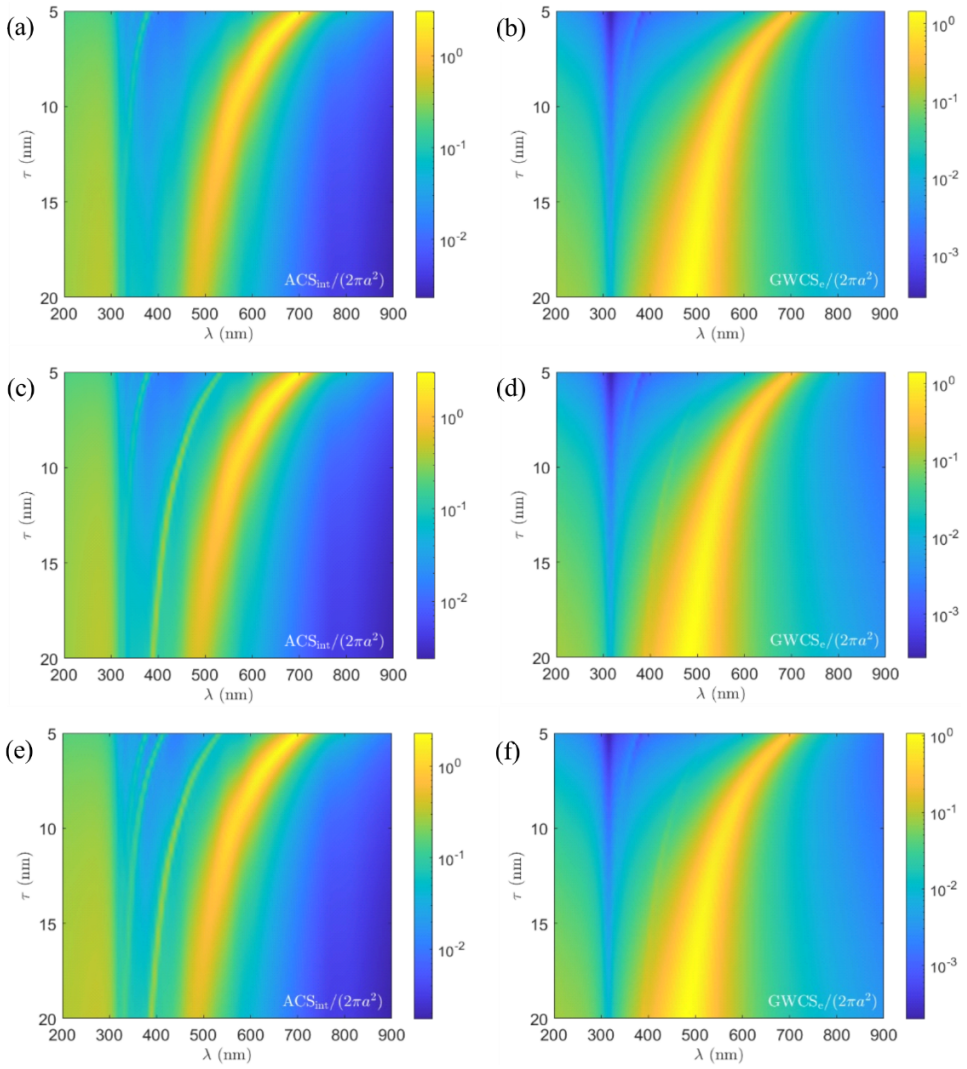

Fig. 10. Plane-wave scattering from a silver disk of radius $a = 50$ nm in a lossless dielectric plate of relative permittivity $\varepsilon_r = 2.25$. Behavior in the optical range and for varying values of the structure thickness, τ, of $\mathrm{ACS_{int}}$ and $\mathrm{GWCS_e}$ for: (a) and (b) normal incidence, (c) and (d) TE incidence with incidence angles $\theta_i = 30°$ and $\phi_i = 0°$, (e) and (f) TM incidence with incidence angles $\theta_i = 30°$ and $\phi_i = 0°$.

associated with different azimuth harmonic orders, i.e., of the kind P_{mn} for $m \neq 1$. These new peaks are marked in Figs. 7(d) and 8(d) and will be discussed in the following. By comparing Figs. 5(d), 7(d), and 8d, it is worth observing that a smaller thickness allows for a better distinction between the resonance behavior for the normal and oblique TE and TM incidences due to the higher quality factors of the involved plasmon modes.

To conclude, in Figs. 9 and 10, a detailed analysis of the visible-range plasmon mode resonances of a silver disk of radius $a = 50$ nm in a lossless dielectric plate of relative dielectric permittivity $\varepsilon_r = 2.25$, for normal incidence, and oblique TE and TM incidences of the plane wave with $\theta_i = 30°$ and $\phi_i = 0°$, is presented. In Fig. 9(a), we show the spectra of $\mathrm{ACS_{int}}$ for structure thickness $\tau = 5$ nm, where we mark the resonance wavelengths. As stated before, with such

Optics EXPRESS

a choice the resonances excited for the normal and oblique TE and TM incidences are clearly identified and distinguished. The most pronounced peak is at the wavelength 701.7 nm for all the cases examined, i.e., for normal and oblique TE and TM incidences. It is related to the fundamental plasmon-mode resonance of the silver disk for $m = 1$, i.e., P_{11}. Another, less pronounced, peak at the wavelength 378.8 nm can be also observed in all the cases examined. It is associated with the higher order plasmon mode resonance with the same azimuthal behavior, P_{12}. Unlike the normal incidence case, a new peak at the wavelength 533.4 nm, associated with the plasmon mode resonance P_{21}, can be observed for both the TE and TM oblique incidence. Moreover, an extra peak at the wavelength 415.0 nm, related to the plasmon mode resonance P_{01}, arises only at the oblique TM incidence because, for the TE incidence, the zero-order azimuthal harmonic of the component of the total field along the z axis vanishes and, hence, a plasmon wave cannot be supported. For the sake of completeness, the amplitude of the total electric field for all the resonance wavelengths marked in Fig. 9(a) are reconstructed in Figs. 9(b) to 9(e) for the oblique TM incidence of the plane wave with $\theta_i = 30°$ and $\phi_i = 0°$. It is worth observing that a larger field enhancement is obtained for the larger values of the resonance wavelengths. This, in turn, is directly related to the larger values of the quality factors of the plasmon modes that, according to the Drude model, have the order of $\Re\{-\varepsilon_r'(\lambda_{mn}^P)\}/\Im\{\varepsilon_r'(\lambda_{mn}^P)\} \sim O(\lambda_{mn}^P)^2$ in the visible range, with λ_{mn}^P denoting the resonance wavelength on the mode P_{mn}. Moreover, in order to qualitatively appreciate the low of variation of the resonance wavelengths as a function of the structure thickness, the behavior of $\mathrm{GWCS_e}$ and $\mathrm{ACS_{int}}$, for varying values of the wavelength in the visible range and of the thickness in the range 5-20 nm, are provided in Fig. 10. The explained above properties of the "short-range" hybrid surface plasmon wave of thin metal layer allow to reach the conclusion that $\lambda_{mn}^P = const\frac{a}{\tau}$. This type of behavior is well visible in Fig. 10, although exact values of the plasmon-mode resonance frequencies depend on the parameters of the dielectric plate, in which the hole, sealed with the silver disk, is cut.

7. Conclusion

A new Optical Theorem has been proposed for the 3-D scattering from a locally perturbed resistive plane and dielectric lossless or lossy plate. The proposed approach takes into account the outgoing cylindrical guided waves excited due to the diffraction from the inhomogeneity, by integrating them with the classical outgoing spherical wave, satisfying the Silver-Muller radiation condition. Moreover, the analysis of the absorption is carried out in a "perturbative sense" by means of the introduction of a new quickly evaluable parameter whose physical meaning is inferred by the conservation of power principle. The proposed formulation has been successfully applied to the analysis of the power budget of the plane-wave scattering from a thin dielectric plate with a circular hole, sealed with a silver nanodisk, in the visible-light range. Such a disk resonates at the wavelengths of the plasmon modes. Our analysis has demonstrated that, in the disk resonances, the cylindrical guided waves of the dielectric plate can carry the power, comparable with the power scattered into the free-space half-spaces.

Appendix A

This Appendix is aimed at demonstrating Eq. (10) for $\Re\{R\}>0$, being the generalization to the case $\Re\{R\} = 0$ straightforward, and Eq. (12).

The function $\underline{\tilde{E}}_{\lessgtr}^{\mathrm{diffr}}(w,\psi)e^{-\mathrm{j}\underline{k}_{\lessgtr}(w,\psi)\cdot\underline{r}}w$ is analytic in the regions of the complex plane $w = w_R + \mathrm{j}w_I$ delimited by the contours C_l with $l = 1, 2$ sketched in Figs. 11 except for $w = w_P^+$ where it has a simple pole singularity. Moreover, for $w \to \infty$, such a function exhibits an asymptotic exponential decay almost everywhere in the half-plane $w_I \geq 0$ ($w_I \leq 0$) for $c_{\phi-\psi} \leq 0$ ($c_{\phi-\psi} \geq 0$).

Optics EXPRESS

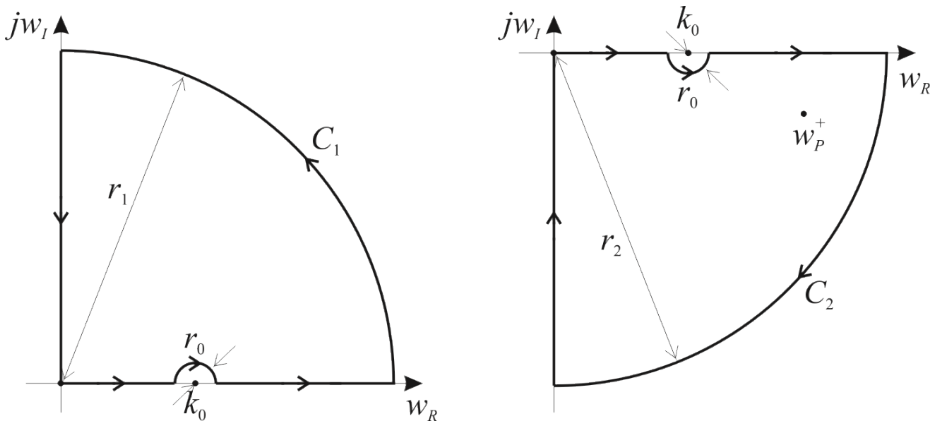

Fig. 11. Integration paths in the complex plane.

By means of Cauchy's integral and residue theorems, it is possible to write

$$\lim_{\substack{r_0\to 0\\ r_1\to+\infty}} \oint_{C_1} \underline{\tilde{E}}_{\lessgtr}^{\mathrm{diffr}}(w,\psi) e^{-\mathrm{j}\underline{k}_{\lessgtr}(w,\psi)\cdot\underline{r}} w dw = 0, \tag{40a}$$

$$\lim_{\substack{r_0\to 0\\ r_2\to+\infty}} \oint_{C_2} \underline{\tilde{E}}_{\lessgtr}^{\mathrm{diffr}}(w,\psi) e^{-\mathrm{j}\underline{k}_{\lessgtr}(w,\psi)\cdot\underline{r}} w dw = -2\pi\mathrm{j}\underline{\tilde{E}}_{P,\lessgtr}^{\mathrm{diffr}}(\psi) e^{-\mathrm{j}\underline{k}_{\lessgtr}(w_P^+,\psi)\cdot\underline{r}} w_P^+. \tag{40b}$$

For $c_{\phi-\psi} \le 0$, by invoking Jordan's lemma and observing that the contour C_1 detours around the branch point k_0 like the contour C in Fig. 2(a), i.e., in clockwise sense, Eq. (40a) can be equivalently written as follows:

$$\int_C \underline{\tilde{E}}_{\lessgtr}^{\mathrm{diffr}}(w,\psi) e^{-\mathrm{j}\underline{k}_{\lessgtr}(\mathrm{w},\psi)\cdot\underline{r}} w dw = -\int_0^{+\infty} \underline{\tilde{E}}_{\lessgtr}^{\mathrm{diffr}}(\mathrm{j}w_I,\psi)\, e^{-\mathrm{j}\underline{k}_{\lessgtr}(\mathrm{j}w_I,\psi)\cdot\underline{r}} w_I dw_I. \tag{41}$$

On the other hand, for $c_{\phi-\psi} \ge 0$, according to Jordan's lemma and noting that the contour C_2 detours around k_0 counterclockwise, the following equivalent expression for Eq. (40b) can be obtained:

$$\begin{aligned}
&\int_C \underline{\tilde{E}}_{\lessgtr}^{\mathrm{diffr}}(w,\psi) e^{-\mathrm{j}\underline{k}_{\lessgtr}(w,\psi)\cdot\underline{r}} w dw \\
&= \int_0^{k_0} \left(\underline{\tilde{E}}_{\lessgtr}^{\mathrm{diffr}}(w_R,\psi) e^{-\mathrm{j}\underline{k}_{\lessgtr}(w_R,\psi)\cdot\underline{r}} - \underline{\tilde{E}}_{-,\lessgtr}^{\mathrm{diffr}}(w_R,\psi) e^{-\mathrm{j}\underline{k}_{-,\lessgtr}(w_R,\psi)\cdot\underline{r}} \right) w_R dw_R \\
&- \int_0^{+\infty} \underline{\tilde{E}}_{-,\lessgtr}^{\mathrm{diffr}}(-\mathrm{j}w_I,\psi) e^{-\mathrm{j}\underline{k}_{-,\lessgtr}(-\mathrm{j}w_I,\psi)\cdot\underline{r}} w_I dw_I \\
&- 2\pi\mathrm{j}\underline{\tilde{E}}_{P,\lessgtr}^{\mathrm{diffr}}(\psi) e^{-\mathrm{j}\underline{k}_{\lessgtr}(w_P^+,\psi)\cdot\underline{r}} w_P^+.
\end{aligned} \tag{42}$$

Since

$$\begin{aligned}
\underline{E}^{\mathrm{diffr}}(\underline{r}) &= \int_0^{2\pi} \int_C \underline{\tilde{E}}_{\lessgtr}^{\mathrm{diffr}}(w,\psi) e^{-\mathrm{j}\underline{k}_{\lessgtr}(w,\psi)\cdot\underline{r}} w dw d\psi \\
&= \int_{c_{\phi-\psi}\ge 0} \int_C \underline{\tilde{E}}_{\lessgtr}^{\mathrm{diffr}}(w,\psi) e^{-\mathrm{j}\underline{k}_{\lessgtr}(w,\psi)\cdot\underline{r}} w dw d\psi \\
&+ \int_{c_{\phi-\psi}\le 0} \int_C \underline{\tilde{E}}_{\lessgtr}^{\mathrm{diffr}}(w,\psi) e^{-\mathrm{j}\underline{k}_{\lessgtr}(w,\psi)\cdot\underline{r}} w dw d\psi,
\end{aligned} \tag{43}$$

Optics EXPRESS

by using Eqs. (41) and (42), the diffracted electric field can be simply written as follows:

$$\begin{aligned}\underline{E}^{\text{diffr}}(\underline{r}) = &\int\limits_{c_{\phi-\psi}\geq 0}\Bigg[\int\limits_{0}^{k_0}\left(\underline{\tilde{E}}^{\text{diffr}}_{\lessgtr}(w_R,\psi)\,e^{-\text{j}\underline{k}_{\lessgtr}(w_R,\psi)\cdot\underline{r}} - \underline{\tilde{E}}^{\text{diffr}}_{-,\lessgtr}(w_R,\psi)\,e^{-\text{j}\underline{k}_{-,\lessgtr}(w_R,\psi)\cdot\underline{r}}\right)w_R dw_R\\ &-\int\limits_{0}^{+\infty}\underline{\tilde{E}}^{\text{diffr}}_{-,\lessgtr}(-\text{j}w_I,\psi)\,e^{-\text{j}\underline{k}_{-,\lessgtr}(-\text{j}w_I,\psi)\cdot\underline{r}}w_I dw_I\\ &-2\pi\text{j}\underline{\tilde{E}}^{\text{diffr}}_{P,\lessgtr}(\psi)\,e^{-\text{j}\underline{k}_{\lessgtr}(w_P^+,\psi)\cdot\underline{r}}w_P^+\Bigg]d\psi\\ &-\int\limits_{c_{\phi-\psi}\leq 0}\int\limits_{0}^{+\infty}\underline{\tilde{E}}^{\text{diffr}}_{\lessgtr}(\text{j}w_I,\psi)\,e^{-\text{j}\underline{k}_{\lessgtr}(\text{j}w_I,\psi)\cdot\underline{r}}w_I dw_I d\psi.\end{aligned} \tag{44}$$

On the other hand, according to Eqs. (6), (7), and (8), the integration domain of the last integral at the right-hand side of Eq. (44) can be changed as follows:

$$\begin{aligned}&\int\limits_{c_{\phi-\psi}\leq 0}\int\limits_{0}^{+\infty}\underline{\tilde{E}}^{\text{diffr}}_{\lessgtr}(\text{j}w_I,\psi)\,e^{-\text{j}\underline{k}_{\lessgtr}(\text{j}w_I,\psi)\cdot\underline{r}}w_I dw_I d\psi\\ &=\int\limits_{c_{\phi-\psi}\geq 0}\int\limits_{0}^{+\infty}\underline{\tilde{E}}^{\text{diffr}}_{\lessgtr}(\text{j}w_I,\psi+\pi)\,e^{-\text{j}\underline{k}_{\lessgtr}(\text{j}w_I,\psi+\pi)\cdot\underline{r}}w_I dw_I d\psi\\ &=\int\limits_{c_{\phi-\psi}\geq 0}\int\limits_{0}^{+\infty}\underline{\tilde{E}}^{\text{diffr}}_{\lessgtr}(-\text{j}w_I,\psi)\,e^{-\text{j}\underline{k}_{\lessgtr}(-\text{j}w_I,\psi)\cdot\underline{r}}w_I dw_I d\psi.\end{aligned} \tag{45}$$

As a result, Eq. (10) can be immediately obtained by substituting Eq. (45) in Eq. (44).

Now, in order to demonstrate Eq. (12), let us consider Eq. (10).

For $r\rightarrow+\infty$ and $\psi\neq 0,\pi$, the integrand $(\underline{\tilde{E}}^{\text{diffr}}_{\lessgtr}(-\text{j}w_I,\psi)e^{-\text{j}\underline{k}_{\lessgtr}(-\text{j}w_I,\psi)\cdot\underline{r}} + \underline{\tilde{E}}^{\text{diffr}}_{-,\lessgtr}(-\text{j}w_I,\psi)\,e^{-\text{j}\underline{k}_{-,\lessgtr}(-\text{j}w_I,\psi)\cdot\underline{r}})w_I$ has an asymptotic exponential decay. Moreover, for $\psi=0,\pi$, the stationary phase method leads to the stationary phase point $w_I=0$ at which such integrand vanishes. Hence, the corresponding integral asymptotically vanishes.

On the other hand, the function $\underline{\tilde{E}}^{\text{diffr}}_{-,\lessgtr}(w_R,\psi)e^{-\text{j}\underline{k}_{-,\lessgtr}(w_R,\psi)\cdot\underline{r}}w_R$ has no stationary phase points, whereas $\underline{\tilde{E}}^{\text{diffr}}_{\lessgtr}(w_R,\psi)e^{-\text{j}\underline{k}_{\lessgtr}(w_R,\psi)\cdot\underline{r}}w_R$ has a stationary phase point for $w_R=k_0 s_\theta$ and $\psi=\phi$. Hence, by means of the stationary phase method, it is simple to show that

$$\begin{aligned}&\int_{c_{\phi-\psi}\geq 0}\int_0^{k_0}\left(\underline{\tilde{E}}^{\text{diffr}}_{\lessgtr}(w_R,\psi)\,e^{-\text{j}\underline{k}_{\lessgtr}(w_R,\psi)\cdot\underline{r}} - \underline{\tilde{E}}^{\text{diffr}}_{-,\lessgtr}(w_R,\psi)\,e^{-\text{j}\underline{k}_{-,\lessgtr}(w_R,\psi)\cdot\underline{r}}\right)w_R dw_R d\psi\\ &\qquad\overset{r\rightarrow+\infty}{\sim}\frac{e^{-\text{j}k_0 r}}{r}\underline{F}(\theta,\phi).\end{aligned} \tag{46}$$

Moreover, due to the stationary phase point of the function $\underline{\tilde{E}}^{\text{diffr}}_{P,\lessgtr}(\psi)e^{-\text{j}\underline{k}_{\lessgtr}(w_P^+,\psi)\cdot\underline{r}}$ for $\psi=\phi$, it is possible to write

$$\int_{c_{\phi-\psi}\geq 0}\underline{\tilde{E}}^{\text{diffr}}_{P,\lessgtr}(\psi)e^{-j\underline{k}_{\lessgtr}(w_P^+,\psi)\cdot\underline{r}}d\psi\overset{\rho\rightarrow+\infty}{\sim}e^{\text{j}\frac{\pi}{4}}\sqrt{\frac{2\left(w_P^{+2}-k_0^2\right)}{\pi w_P^{+3}\rho}}e^{-\text{j}\underline{k}_{\lessgtr}(w_P^+,\phi)\cdot\underline{r}}\underline{F}_{P,\lessgtr}(\phi). \tag{47}$$

According to the considerations detailed above and using Eqs. (46) and (47) in (10), Eq. (12) can be immediately obtained.

Optics EXPRESS

Appendix B

In this Appendix it is demonstrated that the behavior for $\bar{r} \to +\infty$ of the first integral at the left-hand side of Eq. (19) can be expressed in closed form for the incident fields in Eqs. (22) and (32).

Supposing that the incident field is the plane wave in Eq. (22), according to Eq. (26), it is possible to decompose the first integral at the left-hand side of Eq. (19) as follows:

$$\begin{aligned}
&\frac{1}{2}\oint_{\bar{S}} (\underline{E}_0(\underline{r}) \times \underline{H}^{\mathrm{diffr}*}(\underline{r}) + \underline{E}^{\mathrm{diffr}}(\underline{r}) \times \underline{H}_0^*(\underline{r})) \cdot \hat{r} dS \\
&= \frac{1}{2}\int_{\bar{S}_+} (\underline{E}^{\mathrm{inc}}(\underline{r}) \times \underline{H}^{\mathrm{diffr}*}(\underline{r}) + \underline{E}^{\mathrm{diffr}}(\underline{r}) \times \underline{H}^{\mathrm{inc}*}(\underline{r})) \cdot \hat{r} dS \\
&+ \frac{1}{2}\int_{\bar{S}_+} (\underline{E}^{\mathrm{refl}}(\underline{r}) \times \underline{H}^{\mathrm{diffr}*}(\underline{r}) + \underline{E}^{\mathrm{diffr}}(\underline{r}) \times \underline{H}^{\mathrm{refl}*}(\underline{r})) \cdot \hat{r} dS \\
&+ \frac{1}{2}\int_{\bar{S}_-} (\underline{E}^{\mathrm{tr}}(\underline{r}) \times \underline{H}^{\mathrm{diffr}*}(\underline{r}) + \underline{E}^{\mathrm{diffr}}(\underline{r}) \times \underline{H}^{\mathrm{tr}*}(\underline{r})) \cdot \hat{r} dS,
\end{aligned} \tag{48}$$

where $\bar{S}_\pm$ denotes the upper/lower half-sphere. For $\bar{r} \to +\infty$, it is simple to show that the integrand of the first integral has no stationary phase points among the integration directions, whereas the integrands of the second and third integrals have stationary phase points along the specular with respect to the incident direction, $(\theta_i, \phi_i \pm \pi)$, and the forward direction, $(\pi - \theta_i, \phi_i \pm \pi)$, respectively. Since $\theta_i < \pi/2$, the cylindrical guided wave exhibits an exponential decay along such directions (independently of the plane resistivity R), and, hence, only the spherical wave asymptotically contributes to the integral. Because of these considerations, Eq. (27) can be readily obtained by means of the stationary phase method.

If the incident field is the plane guided wave in Eq. (32), according to Eqs. (12) and (14), the first integral at the left-hand side of Eq. (19) can be decomposed as follows:

$$\begin{aligned}
&\frac{1}{2}\Re\left\{\oint_{\bar{S}} (\underline{E}_0(\underline{r}) \times \underline{H}^{\mathrm{diffr}*}(\underline{r}) + \underline{E}^{\mathrm{diffr}}(\underline{r}) \times \underline{H}_0^*(\underline{r})) \cdot \hat{r} dS\right\} \\
&= \frac{1}{2}\Re\left\{\oint_{\bar{S}} (\underline{E}_0(\underline{r}) \times \underline{H}_{\mathrm{sph}}^{\mathrm{diffr}*}(\underline{r}) + \underline{E}_{\mathrm{sph}}^{\mathrm{diffr}}(\underline{r}) \times \underline{H}_0^*(\underline{r})) \cdot \hat{r} dS\right\} \\
&+ \frac{1}{2}\Re\left\{\oint_{\bar{S}} (\underline{E}_0(\underline{r}) \times \underline{H}_{\mathrm{cyl}}^{\mathrm{diffr}*}(\underline{r}) + \underline{E}_{\mathrm{cyl}}^{\mathrm{diffr}}(\underline{r}) \times \underline{H}_0^*(\underline{r})) \cdot \hat{r} dS\right\}
\end{aligned} \tag{49}$$

For $\bar{r} \to +\infty$, it can be demonstrated that both the integrands at the right-hand side have two stationary phase points along the backward and the forward directions, i.e., $(\pi/2, \phi_i)$ and $(\pi/2, \phi_i \pm \pi)$, respectively. However, according to Eqs. (12–14), it is simple to conclude that the integrand associated with the spherical wave vanishes for $\theta = \pi/2$, and it is possible to demonstrate that the integrand associated with the cylindrical guided wave is non-vanishing only along the forward direction and only if the involved cylindrical and plane guided waves are both TM/TE with respect to the propagation direction. Based on these considerations, Eq. (34) can be readily obtained by means of the stationary phase method.

Optics EXPRESS

Acknowledgments. O.I.N. acknowledges the support of the Institute of International Education's Scholar Rescue Fund and the hospitality of the Institute of Electronics and Numerical Technologies of the University of Rennes.

Disclosures. The authors declare no conflicts of interest.

Data availability. Data underlying the results presented in this paper are not publicly available at this time but may be obtained from the authors upon reasonable request.

References

1. R. G. Newton, "Optical theorem and beyond," Am. J. Phys. **44**(7), 639–642 (1976).
2. D. Halliday and A. Curtis, "Generalized optical theorem for surface waves and layered media," Phys. Rev. E **79**(5), 056603 (2009).
3. M. Venkatapathi, "Emitter near an arbitrary body: Purcell effect, optical theorem and the Wheeler–Feynman absorber," J. Quant. Spectrosc. Rad. Transfer **113**(13), 1705–1711 (2012).
4. A. Small, J. Fung, and V. N. Manoharan, "Generalization of the optical theorem for light scattering from a particle at a planar interface," J. Opt. Soc. Am. A **30**(12), 2519–2525 (2013).
5. E.A. Marengo and J. Tu, "Generalized optical theorem in the time domain," Progress In Electromagn. Res. B **65**, 1–18 (2016).
6. Y. Ivanenko, M. Gustafsson, and S. Nordebo, "Optical theorems and physical bounds on absorption in lossy media," Opt. Express **27**(23), 34323–34342 (2019).
7. K. Takayanagi and M. Kurino, "Generalized optical theorem," Prog. Theor. Exp. Phys. **2023**(7), 073A02 (2023).
8. G. Mie, "Contributions to the optics of turbid media, particularly of colloidal metal solutions," Annalen der Physik (Leipzig) **330**, 377–445 (1908).
9. H. C. Van De Hulst, "On the attenuation of plane waves by obstacles of arbitrary size and form," Physica **15**(8-9), 740–746 (1949).
10. D. S. Jones, *The Theory Electromagnetism* (Pergamon, 1964).
11. M. I. Mishchenko, "The electromagnetic optical theorem revisited," J. Quantitat. Spectroscopy Rad. Transfer **101**(3), 404–410 (2006).
12. A. Alù and N. Engheta, "How does zero forward-scattering in magnetodielectric nanoparticles comply with the optical theorem?" J. Nanophotonics **4**(1), 041590 (2010).
13. E. I. Smotrova, V. O. Byelobrov, T. M. Benson, *et al.*, "Optical theorem helps understand thresholds of lasing in microcavities with active regions," IEEE J. Quant. Electron. **47**(1), 20–30 (2011).
14. P. G. Petropoulos and G. A. Kriegsmann, "Optical theorems for electromagnetic scattering by inhomogeneities in layered media," IEEE Trans. Antennas Propag. **39**(8), 1119–1124 (1991).
15. A. I. Nosich, "Radiation conditions, limiting absorption principle, and general relations in open waveguide scattering," J. Electromag. Waves Applicat. **8**(3), 329–353 (1994).
16. M. Gustafsson, I. Vakili, S. E. Bayer Keskin, *et al.*, "Optical theorem and forward scattering sum rule for periodic structures," IEEE Trans. Antennas Propag. **60**(8), 3818–3826 (2012).
17. M. Lucido and A. I. Nosich, "Analytical regularization approach to plane wave diffraction from circular hole in infinite resistive plane," IEEE Trans. Antennas Propag. **71**(8), 6878–6892 (2023).
18. M. Lucido, "Absorption by a holed resistive plane: a new optical theorem formulation," in *Int. Conf. Electromagnetics in Advanced Applicat.* (2023), pp. 497–500.
19. E. Bleszynski, M. Bleszynski, and T. Jaroszewicz, "Surface-integral equations for electrmagnetic scattering from impenetrable and penetrable sheets," IEEE Antennas Propag. Mag. **35**(6), 14–25 (1993).
20. I. M. Braver, P. S. Fridberg, K. L. Garb, *et al.*, "Edge conditions for the junction of two resistive half-planes with different surface impedances," in *28th Convention of Electrical and Electronics Engineers in Israel* (IEEE, 2014), pp. 1–4.
21. D. S. Jones, "Removal of an inconsistency in the theory of diffraction," Math. Proc. Cambridge Philos. Soc. **48**(4), 733–741 (1952).
22. M. Lucido, G. Chirico, M. D. Migliore, *et al.*, "Plane-wave diffraction from resistive-filled circular hole in infinite resistive plane: an analytically regularizing approach," Appl. Sci. **13**(13), 7465 (2023).
23. A. Karlsson, "Approximate boundary conditions for thin structures," IEEE Trans. Antennas Propag. **57**(1), 144–148 (2009).
24. P. B. Johnson and R. W. Christy, "Optical constants of the noble metals," Phys. Rev. B **6**(12), 4370–4379 (1972).
25. G. Della Valle, T. Søndergaard, and S. I. Bozhevolnyi, "Plasmon-polariton nano-strip resonators: from visible to infra-red," Opt. Express **16**(10), 6867–6876 (2008).